

Towards Analyzing Semantic Robustness of Deep Neural Networks

Abdullah Hamdi and Bernard Ghanem

King Abdullah University of Science and Technology (KAUST), Thuwal, Saudi Arabia
{abdullah.hamdi, bernard.ghanem}@kaust.edu.sa

Abstract. Despite the impressive performance of Deep Neural Networks (DNNs) on various vision tasks, they still exhibit erroneous high sensitivity toward semantic primitives (*e.g.* object pose). We propose a theoretically grounded analysis for DNNs robustness in the semantic space. We qualitatively analyze different DNNs semantic robustness by visualizing the DNN global behavior as semantic maps and observe interesting behavior of some DNNs. Since generating these semantic maps does not scale well with the dimensionality of the semantic space, we develop a bottom-up approach to detect robust regions of DNNs. To achieve this, we formalize the problem of finding robust semantic regions of the network as optimization of integral bounds and develop expressions for update directions of the region bounds. We use our developed formulations to quantitatively evaluate the semantic robustness of different famous network architectures. We show through extensive experimentation that several networks, though trained on the same dataset and while enjoying comparable accuracy, they do not necessarily perform similarly in semantic robustness. For example, InceptionV3 is more accurate despite being less semantically robust than ResNet50. We hope that this tool will serve as the first milestone towards understanding the semantic robustness of DNNs.

1 Introduction

As a result of recent advances in machine learning and computer vision, deep neural networks (DNNs) have become an essential part of our lives. DNNs are used to suggest articles to read, detect people in surveillance cameras, automate big machines in factories, and even diagnose X-rays for patients in hospitals. So, what is the catch here? These DNNs struggle with a detrimental weakness on specific naive scenarios, despite having strong on-average performance. Fig. 1 shows how a small perturbation in the view angle of the teapot object results in a drop in InceptionV3 [37] confidence score from 100% to almost 0%. The *softmax* confidence scores are plotted against one semantic parameter (*i.e.* the azimuth angle around the teapot) and it fails in such a simple task. Similar behaviors are consistently observed across different DNNs (trained on ImageNet [32]) as noted by other concurrent works [1].

The code is available at <https://github.com/ajhamdi/semantic-robustness>.

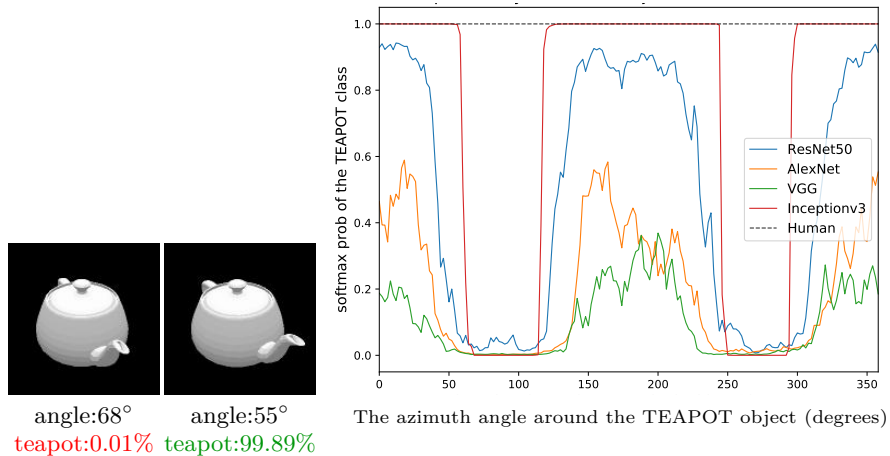


Fig. 1: **Semantic Robustness of Deep Networks.** Trained neural networks can perform poorly when subject to small perturbations in the semantics of the image. (left): We show how perturbing the azimuth viewing angle of a simple *teapot* object can dramatically affect the score of a pretrained InceptionV3 [37] for the *teapot* class. (right): We plot the softmax confidence scores of different DNNs on the same *teapot* object viewed from 360 degrees around the object. For comparison, lab researchers identified the object from all angles.

Furthermore, because DNNs are not easily interpretable, they work well without a complete understanding of *why* they behave in such a manner. A whole research direction is dedicated to studying and analyzing DNNs. Examples of such analysis include activation visualization [9,41,26], noise injection [12,27,3], and studying the effect of image manipulation on DNNs [14,14,13]. By leveraging a differentiable renderer \mathbf{R} and evaluating rendered images for different semantic parameters \mathbf{u} , we provide a new lens of semantic robustness analysis for such DNNs as illustrated in Fig. 2. These Network Semantic Maps (NSM) demonstrate unexpected behavior of some DNNs, in which adversarial regions lie inside a very confident region of the semantic space. This constitutes a “trap” that is hard to detect without such analysis and can lead to catastrophic failure for the DNN.

Recent work in adversarial network attacks explores DNN sensitivity and performs gradient updates to derive targeted perturbations [39,15,6,24]. In practice, such attacks are less likely to naturally occur than semantic attacks, such as changes in camera viewpoint and lighting conditions. The literature on semantic attacks is sparser, since they are more subtle and challenging to analyze [25,17,42,1]. This is due to the fact that we are unable to distinguish between failure cases that result from the network structure, and learning, or from the data bias [40]. Current methods for adversarial semantic attacks either work on individual examples [1], or try to find distributions but rely on sampling methods, which do not scale with dimensionality [17]. We present a novel approach to find robust/adversarial regions in the n-dimensional semantic space. The proposed

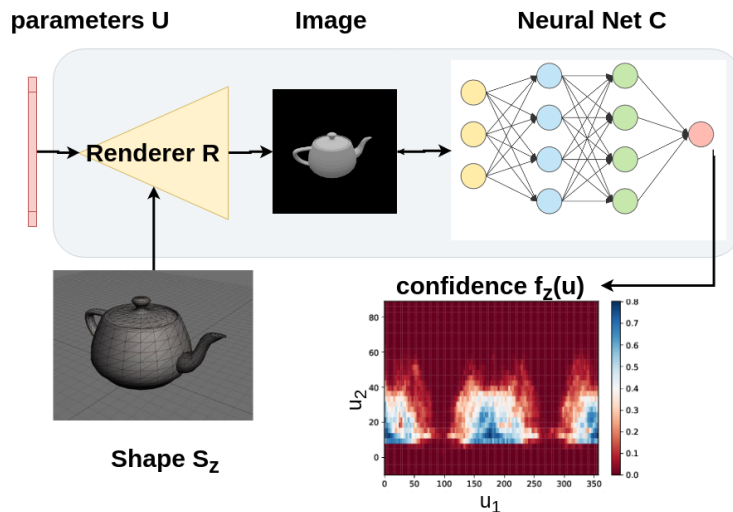


Fig. 2: **Analysis Pipeline:** We leverage neural mesh renderer R [21] to render shape S_z of class z according to semantic scene parameters \mathbf{u} . The resulting image is passed to trained network C that is able to identify the class z . The behaviour of the softmax score at label z (dubbed $f_z(\mathbf{u})$) is analyzed for different parameters \mathbf{u} and for the specific shape S_z . In our experiments, we pick u_1 and u_2 to be the azimuth and elevation angles, respectively.

method scales better than sampling-based methods [17]. We use this method to quantify semantic robustness of popular DNNs on a collected dataset.

Contributions. (1) We analyze popular deep networks from a semantic lens showing unexpected behavior in the 1D and 2D semantic space. (2) We develop a novel bottom-up approach to detect robust/adversarial regions in the semantic space of a DNN, which scales well with increasing dimensionality. The method specifically optimizes for the region’s bounds in semantic space (around a point of interest), such that the continuous region offers semantic parameters that confuse the network. (3) We develop a new metric to quantify semantic robustness of DNNs that we dub Semantic Robustness Volume Ratio (SRVR), and we use it to benchmark popular DNNs on a collected dataset.

2 Related Work

2.1 Understanding Deep Neural Networks

There are different lenses to analyze DNNs depending on the purpose of analysis. A popular line of work tries to visualize the network hidden layers by inverting the activations to get a visual image that represents a specific activation [9,26,41]. Others observe the behavior of these networks under injected noise [12,2,4,16,38,3]. Geirhos *et. al.* show that changing the texture of the object while keeping the

borders can hugely deteriorate the recognizability of the object by the DNN [14]. More closely related to our work is the work of Fawzi *et. al.*, which shows that geometric changes in the image greatly affect the performance of the classifier [13]. The work of Engstorn *et. al.* [11] studies the robustness of a network under natural 2D transformations (*i.e.* translation and planar rotation).

2.2 Adversarial Attacks on Deep Neural Networks

Pixel-based Adversarial Attacks. The way that DNNs fail for some noise added to the image motivated the adversarial attacks literature. Several works formulate attacking neural networks as an optimization on the input pixels [39,15,24,28,6]. However, all these methods are limited to pixel perturbations and only fool classifiers, while we consider more general cases of attacks, *e.g.* changes in camera viewpoint to fool a DNN by finding adversarial regions. Most attacks are white-box attacks, in which the attack algorithm has access to network gradients. Another direction of adversarial attacks treats the classifier as a black-box, where the adversary can only probe the network and get a score from the classifier without backpropagating through the DNN [29,8]. We formulate the problem of finding the robust/adversarial region as an optimization of the corners of a hyper-rectangle in the semantic space for both black-box and white-box attacks.

Semantic Adversarial Attacks. Other works tried to move away from pixel perturbation to semantic 3D scene parameters and 3D attacks [42,17,1,25,18]. Zeng *et. al.* [42] generate attacks on deep classifiers by perturbing scene parameters like lighting and surface normals. Hamdi *et. al.* propose generic adversarial attacks that incorporate semantic and pixel attacks, in which an adversary is sampled from some latent distribution that is produced from a GAN trained on example semantic adversaries [17]. However, their work used a sampling-based approach to learn these adversarial regions, which does not scale with the dimensionality of the problem. Another recent work by Alcorn *et. al.* [1] tries to fool trained DNNs by changing the pose of the object. They used the Neural Mesh renderer (NMR) by Kato *et. al.* [22] to allow for a fully differentiable pipeline that performs adversarial attacks based on the gradients to the parameters. Our work differs in that we use NMR to obtain gradients to the parameters \mathbf{u} not to attack the model, but to detect and quantify the robustness of different networks as shown in Section 4.4. Furthermore, Dreossi *et. al.* [10] used adversarial training in the semantic space for self-driving, whereas Liu *et. al.* [25] proposed a differentiable renderer to perform parametric attacks and the *parametric-ball* as an evaluation metric for physical attacks. The work by Shu *et. al.* [34] used an RL agent and a Bayesian optimizer to assess the DNNs behaviour under good/bad physical parameters for the network. While we share similar insights as [34], we try to study the global behaviour of DNNs as collections of regions, whereas [34] tries to find individual points that pose difficulty for the DNN.

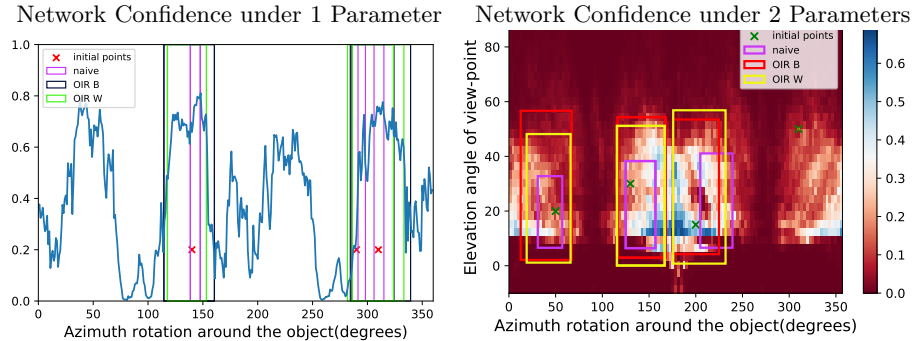


Fig. 3: **Semantic Robust Region Finding:** We find robust regions of semantic parameters for Rsnnet50 [19] and for a *bathub* object by the three bottom-up formulations (naive , OIR_W , and OIR_B). (*left*): Semantic space is 1D (azimuth angle of camera) with three initial points. (*right*): Semantic space is 2D (azimuth angle and elevation angle of camera) with four initial points. We note that the naive approach usually predicts smaller regions, while the OIR formulations find more comprehensive regions.

2.3 Optimizing Integral Bounds

Naive Approach. To develop an algorithm for robust region finding, we adopt an idea from weakly supervised activity detection in videos by Shou *et. al.* [33]. The idea is to find bounds that maximize the inner average of a continuous function while minimizing the outer average in a region. This is achieved because optimizing the bounds to exclusively maximize the area can lead to diverging bounds of $\{-\infty, \infty\}$. To solve the issue of diverging bounds, the following naive formulation is to simply regularize the loss by adding a penalty on the region size. The expressions for the loss of $n=1$ dimension is: $L = -\text{Area}_{\text{in}} + \frac{\lambda}{2} |b - a|_2^2 = \int_a^b f(u)du + \frac{\lambda}{2} |b - a|_2^2$, where $f : \mathbb{R}^1 \rightarrow (0, 1)$ is the function of interest and (a, b) are the left and right bounds respectively and λ is a hyperparameter. The update directions to minimize the loss are: $\frac{\partial L}{\partial a} = f(a) - \lambda(b - a)$; $\frac{\partial L}{\partial b} = -f(b) + \lambda(b - a)$. The regularizer will prevent the region from growing to ∞ and the best bounds will be found if the loss is minimized with gradient descent or any similar approach.

Trapezoidal Approximation. To extend the naive approach to n -dimensions, we face more integrals in the update directions (hard to compute). Therefore, we deploy the following first-order trapezoid approximation of definite integrals. The Newton-Cotes formula for numerical integration [36] states that: $\int_a^b f(u)du \approx (b - a) \frac{f(a) + f(b)}{2}$. An asymptotic error estimate is given by $-\frac{(b-a)^2}{48} [f'(b) - f'(a)] + \mathcal{O}(\frac{1}{8})$. So, as long as the derivatives are bounded by some Lipschitz constant \mathbb{L} , then the error becomes bounded such that $|\text{error}| \leq \mathbb{L}(b - a)^2$.

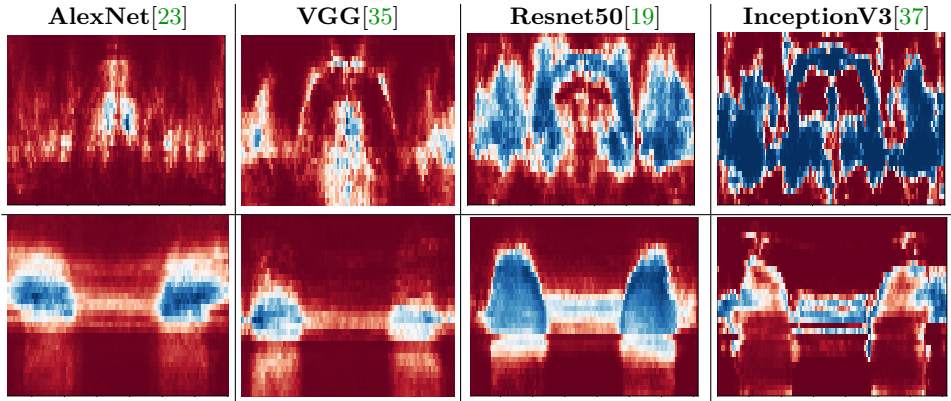


Fig. 4: **Network Semantic Maps**: We plot the 2D semantic maps (as in Fig. 3 right) of four different networks on two shapes of a *chair* class (*top*) and *cup* class (*bottom*). InceptionV3 is very confident about its decision, but at the cost of creating semantic “traps”, where sharp performance degradation happens in the middle of a robust region. This behaviour is more apparent for complex shapes (*e.g.* the chair in *top* row).

3 Methodology

Typical adversarial pixel attacks involve a neural network \mathbf{C} (*e.g.* classifier or detector) that takes an image $\mathbf{x} \in [0, 1]^d$ as input and outputs a multinoulli distribution over K class labels with softmax values $[l_1, l_2, \dots, l_K]$, where l_j is the softmax value for class j . The adversary (attacker) tries to produce a perturbed image $\mathbf{x}' \in [0, 1]^d$ that is as close as possible to \mathbf{x} , such that \mathbf{x} to \mathbf{x}' have different class predictions through \mathbf{C} . In this work, we consider a more general case where we are interested in parameters $\mathbf{u} \in \Omega \subset \mathbb{R}^n$, a latent parameter that generates the image via a scene generator (*e.g.* a renderer function \mathbf{R}). This generator/renderer takes the parameter \mathbf{u} and an object shape \mathbf{S} of a class that is identified by \mathbf{C} . Ω is the continuous semantic space for the parameters that we intend to study. The renderer creates the image $\mathbf{x} \in \mathbb{R}^d$, and then we study the behavior of a classifier \mathbf{C} of that image across multiple shapes and multiple popular DNN architectures. Now, this function of interest is defined as follows:

$$f(\mathbf{u}) = \mathbf{C}_z(\mathbf{R}(\mathbf{S}_z, \mathbf{u})) , \quad 0 \leq f(\mathbf{u}) \leq 1 \quad (1)$$

where z is a class label of interest to study and we observe the network score for that class by rendering a shape \mathbf{S}_z of the same class. The shape and class labels are constants and only the parameters \mathbf{u} vary for f during analysis.

3.1 Region Finding as an Operator

We can visualize the function in Eq (1) for any shape \mathbf{S}_z as long as the DNN can identify the shape at some region in the semantic space Ω of interest, as we

show in Fig. 1. However, plotting these figures is expensive and the complexity of plotting them increases exponentially with a big base. The complexity of plotting these plots of semantic maps, which we call Network Semantic Maps (NSM), is N for $n = 1$, where N is the number of samples needed for that dimension to be fully characterized. The complexity is N^2 for $n = 2$, and we can see that for a general dimension n , the complexity of plotting the NMS to adequately fill the semantic space Ω is N^n . This number is intractable even if we have only moderate dimensionality. To tackle this issue, we use a bottom-up approach to detect regions around some initial parameters \mathbf{u}_0 , instead of sampling in the entire space of parameters Ω . Explicitly, we define region finding as an operator Φ that takes the function of interest in Eq (1), initial point in the semantic space $\mathbf{u}_0 \in \Omega$, and a shape \mathbf{S}_z of some class z . The operator will return the hyper-rectangle $\mathbb{D} \subset \Omega$, where the DNN is robust in the region and does not sharply drop the score of the intended class. It also keeps identifying the shape with label z as illustrated in Fig. 4. The robust-region-finding operator is then defined as follows:

$$\begin{aligned} \Phi_{\text{robust}}(f(\mathbf{u}), \mathbf{S}_z, \mathbf{u}_0) = \mathbb{D} = \{\mathbf{u} : \mathbf{a} \leq \mathbf{u} \leq \mathbf{b}\} \\ \text{s.t. } \mathbb{E}_{\mathbf{u} \sim \mathbb{D}}[f(\mathbf{u})] \geq 1 - \epsilon_m, \quad \mathbf{u}_0 \in \mathbb{D}, \quad \text{VAR}[f(\mathbf{u})] \leq \epsilon_v \end{aligned} \quad (2)$$

where the left and right bounds of \mathbb{D} are $\mathbf{a} = [a_1, a_2, \dots, a_n]$ and $\mathbf{b} = [b_1, b_2, \dots, b_n]$, respectively. The two small thresholds (ϵ_m, ϵ_v) are needed to ensure high performance and low variance of the DNN in that robust region. We can define the complementary operator, which finds adversarial regions as:

$$\begin{aligned} \Phi_{\text{adv}}(f(\mathbf{u}), \mathbf{S}_z, \mathbf{u}_0) = \mathbb{D} = \{\mathbf{u} : \mathbf{a} \leq \mathbf{u} \leq \mathbf{b}\} \\ \text{s.t. } \mathbb{E}_{\mathbf{u} \sim \mathbb{D}}[f(\mathbf{u})] \leq \epsilon_m, \quad \mathbf{u}_0 \in \mathbb{D}, \quad \text{VAR}[f(\mathbf{u})] \geq \epsilon_v \end{aligned} \quad (3)$$

We can clearly show that Φ_{adv} and Φ_{robust} are related:

$$\Phi_{\text{adv}}(f(\mathbf{u}), \mathbf{S}_z, \mathbf{u}_0) = \Phi_{\text{robust}}(1 - f(\mathbf{u}), \mathbf{S}_z, \mathbf{u}_0) \quad (4)$$

So, we can just focus our attention on Φ_{robust} to find robust regions, and the adversarial regions follow directly from Eq (4). We need to ensure that \mathbb{D} has a positive size: $\mathbf{r} = \mathbf{b} - \mathbf{a} > \mathbf{0}$. The volume of \mathbb{D} normalized by the exponent of dimension n is expressed as follows:

$$\text{volume}(\mathbb{D}) = \Delta = \frac{1}{2^n} \prod_{i=1}^n \mathbf{r}_i \quad (5)$$

The region \mathbb{D} can also be defined in terms of the matrix \mathbf{D} of all the corner points $\{\mathbf{d}^i\}_{i=1}^{2^n}$ as follows:

$$\begin{aligned} \text{corners}(\mathbb{D}) = \mathbf{D}_{n \times 2^n} = \left[\mathbf{d}^1 | \mathbf{d}^2 | \dots | \mathbf{d}^{2^n} \right] = \mathbf{1}^T \mathbf{a} + \mathbf{M}^T \odot (\mathbf{1}^T \mathbf{r}) \\ \mathbf{M}_{n \times 2^n} = \left[\mathbf{m}^0 | \mathbf{m}^1 | \dots | \mathbf{m}^{2^n-1} \right], \quad \text{where } \mathbf{m}^i = \text{binary}_n(i) \end{aligned} \quad (6)$$

and $\mathbf{1}$ is the all-ones vector of size 2^n , \odot is the Hadamard (element-wise) product of matrices, and \mathbf{M} is a constant masking matrix defined as the permutation matrix of binary numbers of n bits that range from 0 to $2^n - 1$

3.2 Deriving Update Directions

Extending Naive to n -dimensions. We start by defining the function vector $\mathbf{f}_{\mathbb{D}}$ of all function evaluations at all corner points of \mathbb{D} .

$$\mathbf{f}_{\mathbb{D}} = \left[f(\mathbf{d}^1), f(\mathbf{d}^2), \dots, f(\mathbf{d}^{2^n}) \right]^T, \quad \mathbf{d}^i = \mathbf{D}_{:,i} \quad (7)$$

Then, using Trapezoid approximation and Leibniz rule of calculus, the loss expression and the update directions become as follows:

$$\begin{aligned} L(\mathbf{a}, \mathbf{b}) &= - \int \cdots \int_{\mathbb{D}} f(u_1, \dots, u_n) du_1 \dots du_n + \frac{\lambda}{2} |\mathbf{r}|^2 \approx -\Delta \mathbf{1}^T \mathbf{f}_{\mathbb{D}} + \frac{\lambda}{2} |\mathbf{r}|^2 \\ \nabla_{\mathbf{a}} L &\approx 2\Delta \text{diag}^{-1}(\mathbf{r}) \overline{\mathbf{M}} \mathbf{f}_{\mathbb{D}} + \lambda \mathbf{r} \quad ; \quad \nabla_{\mathbf{b}} L \approx -2\Delta \text{diag}^{-1}(\mathbf{r}) \mathbf{M} \mathbf{f}_{\mathbb{D}} - \lambda \mathbf{r} \end{aligned} \quad (8)$$

We show all the derivations for $n \in \{1, 2\}$ and for general n in the **supplement**.

Outer-Inner Ratio Loss (OIR). We introduce an outer region (A, B) with that contains the small region (a, b) . We follow the following assumption to ensure that the outer area is always positive: $A = a - \alpha \frac{b-a}{2}$; $B = b + \alpha \frac{b-a}{2}$. Here, α is the small boundary factor of the outer area to the inner. We formulate the problem as a ratio of outer over inner areas and we try to make this ratio ($L = \frac{\text{Area}_{\text{out}}}{\text{Area}_{\text{in}}}$) as close as possible to 0. We utilize the Dinkelbach technique for solving non-linear fractional programming problems [31] to transform L as follows.

$$\begin{aligned} L &= \frac{\text{Area}_{\text{out}}}{\text{Area}_{\text{in}}} = \text{Area}_{\text{out}} - \lambda \text{Area}_{\text{in}} \\ &= \int_A^B f(a) du - \int_a^b f(a) du - \lambda \int_a^b f(a) du \end{aligned} \quad (9)$$

where $\lambda^* = \frac{\text{Area}_{\text{out}}^*}{\text{Area}_{\text{in}}^*}$ is the Dinkelbach factor that is the best objective ratio.

Black-Box (OIR_B). Here we set $\lambda = 1$ to simplify the problem. This yields the following expression of the loss $L = \text{Area}_{\text{out}} - \text{Area}_{\text{in}} = \int_A^B f(u) du - 2 \int_a^b f(u) du$, which is similar to the area contrastive loss in [33]. The update rules would be $\frac{\partial L}{\partial a} = -(1 + \frac{\alpha}{2})f(A) - \frac{\alpha}{2}f(B) + 2f(a)$; $\frac{\partial L}{\partial b} = (1 + \frac{\alpha}{2})f(B) + \frac{\alpha}{2}f(A) - 2f(b)$. To extend to n -dimensions, we define an outer region \mathbb{Q} that includes the smaller region \mathbb{D} and defined as: $\mathbb{Q} = \{\mathbf{u} : \mathbf{a} - \frac{\alpha}{2}\mathbf{r} \leq \mathbf{u} \leq \mathbf{b} + \frac{\alpha}{2}\mathbf{r}\}$, where $(\mathbf{a}, \mathbf{b}, \mathbf{r})$ are defined as before, while α is defined as the boundary factor of the outer region for all the dimensions. The inner region \mathbb{D} is defined as in Eq (6), while the outer region can be defined in terms of the corner points as follows:

$$\begin{aligned} \text{corners}(\mathbb{Q}) &= \mathbf{Q}_{n \times 2^n} = \left[\mathbf{q}^1 | \mathbf{q}^2 | \dots | \mathbf{q}^{2^n} \right] \\ \mathbf{Q} &= \mathbf{1}^T \left(\mathbf{a} - \frac{\alpha}{2}\mathbf{r} \right) + (1 + \alpha) \mathbf{M}^T \odot (\mathbf{1}^T \mathbf{r}) \end{aligned} \quad (10)$$

Let $\mathbf{f}_{\mathbb{D}}$ be a function vector as in Eq (7) and $\mathbf{f}_{\mathbb{Q}}$ be another function vector evaluated at all possible outer corner points: $\mathbf{f}_{\mathbb{Q}} = [f(\mathbf{q}^1), f(\mathbf{q}^2), \dots, f(\mathbf{q}^{2^n})]^T$, $\mathbf{q}^i = \mathbf{Q}_{:,i}$.

Now, the loss and update directions for the n -dimensional case becomes:

$$\begin{aligned} L(\mathbf{a}, \mathbf{b}) &= \int \cdots \int_{\mathbb{Q}} f(u_1, \dots, u_n) du_1 \dots du_n - 2 \int \cdots \int_{\mathbb{D}} f(u_1, \dots, u_n) du_1 \dots du_n \\ &\approx \Delta \left((1 + \alpha)^n \mathbf{1}^T \mathbf{f}_{\mathbb{Q}} - 2 \mathbf{1}^T \mathbf{f}_{\mathbb{D}} \right) \\ \nabla_{\mathbf{a}} L &\approx 2\Delta \text{diag}^{-1}(\mathbf{r}) \left(2\overline{\mathbf{M}}\mathbf{f}_{\mathbb{D}} - \overline{\mathbf{M}}_{\mathbb{Q}}\mathbf{f}_{\mathbb{Q}} \right); \quad \nabla_{\mathbf{b}} L \approx 2\Delta \text{diag}^{-1}(\mathbf{r}) \left(-2\mathbf{M}\mathbf{f}_{\mathbb{D}} + \mathbf{M}_{\mathbb{Q}}\mathbf{f}_{\mathbb{Q}} \right), \end{aligned} \quad (11)$$

where $\text{diag}(\cdot)$ is the diagonal matrix of the vector argument or the diagonal vector of the matrix argument. $\overline{\mathbf{M}}_{\mathbb{Q}}$ is the outer region scaled mask defined as follows:

$$\overline{\mathbf{M}}_{\mathbb{Q}} = (1 + \alpha)^{n-1} \left(\left(1 + \frac{\alpha}{2}\right)\overline{\mathbf{M}} + \frac{\alpha}{2}\mathbf{M} \right); \quad \mathbf{M}_{\mathbb{Q}} = (1 + \alpha)^{n-1} \left(\left(1 + \frac{\alpha}{2}\right)\mathbf{M} + \frac{\alpha}{2}\overline{\mathbf{M}} \right) \quad (12)$$

White-Box OIR (OIR_W). Here, we present the white-box formulation of Outer-Inner-Ratio. This requires access to the gradient of the function f in order to update the current estimates of the bound. As we show in Section 4, access to gradients enhance the quality of the detected regions. To derive the formulation, We set $\lambda = \frac{\alpha}{\beta}$ in Eq (9), where α is the small boundary factor of the outer area and β is the gradient emphasis factor. Hence, the objective in Eq (9) becomes:

$$\begin{aligned} \arg \min_{a,b} L &= \arg \min_{a,b} \text{Area}_{\text{out}} - \lambda \text{Area}_{\text{in}} \\ &= \arg \min_{a,b} \int_A^a f(u) du + \int_b^B f(u) du - \frac{\alpha}{\beta} \int_a^b f(u) du \\ &= \arg \min_{a,b} \frac{\beta}{\alpha} \int_{a-\alpha\frac{b-a}{2}}^{b+\alpha\frac{b-a}{2}} f(u) du - \left(1 + \frac{\beta}{\alpha}\right) \int_a^b f(u) du \quad (13) \\ \frac{\partial L}{\partial a} &= \frac{\beta}{\alpha} \left(f(a) - f\left(a - \alpha\frac{b-a}{2}\right) \right) \\ &\quad - \frac{\beta}{2} f\left(b + \alpha\frac{b-a}{2}\right) - \frac{\beta}{2} f\left(a - \alpha\frac{b-a}{2}\right) + f(a) \end{aligned}$$

Now, since λ^* should be small for the optimal objective as $\lambda \rightarrow 0$, $\alpha \rightarrow 0$ and hence the derivative in Eq (13) becomes the following:

$$\begin{aligned} \lim_{\alpha \rightarrow 0} \frac{\partial L}{\partial a} &= \frac{\beta}{2} \left((b-a)f'(a) + f(b) \right) + \left(1 - \frac{\beta}{2}\right)f(a) \\ \lim_{\alpha \rightarrow 0} \frac{\partial L}{\partial b} &= \frac{\beta}{2} \left((b-a)f'(b) + f(a) \right) - \left(1 - \frac{\beta}{2}\right)f(b) \end{aligned} \quad (14)$$

We can see that the update rule for a and b depends on the function value **and** the derivative of f at the boundaries a and b respectively, with β controlling the dependence. If $\beta \rightarrow 0$, the update directions in Eq (14) collapse to the unregularized naive update. To extend to n -dimensions, we have to define a term that involves the gradient of the function, *i.e.* the all-corners gradient matrix $\mathbf{G}_{\mathbb{D}}$.

$$\mathbf{G}_{\mathbb{D}} = \left[\nabla f(\mathbf{d}^1) \mid \nabla f(\mathbf{d}^2) \mid \dots \mid \nabla f(\mathbf{d}^{2^n}) \right]^T \quad (15)$$

Algorithm 1: Robust n -dimensional Region Finding for Black-Box DNNs by Outer-Inner Ratios

Requires: Semantic Function of a DNN $f(\mathbf{u})$ in Eq (1), initial semantic parameter \mathbf{u}_0 , number of iterations T , learning rate η , object shape \mathbf{S}_z of class label z , boundary factor α , Small ϵ
 Form constant binary matrices $\mathbf{M}, \overline{\mathbf{M}}, \mathbf{M}_Q, \overline{\mathbf{M}}_Q, \mathbf{M}_D, \overline{\mathbf{M}}_D$
 Initialize bounds $\mathbf{a}_0 \leftarrow \mathbf{u}_0 - \epsilon \mathbf{1}$, $\mathbf{b}_0 \leftarrow \mathbf{u}_0 + \epsilon \mathbf{1}$
 $\mathbf{r}_0 \leftarrow \mathbf{a}_0 - \mathbf{b}_0$, update region volume Δ_0 as in Eq (5)
for $t \leftarrow 1$ **to** T **do**
 form the all-corners function vectors f_D, f_Q as in Eq (7,10)
 $\nabla_{\mathbf{a}} L \leftarrow 2\Delta_{t-1} \text{diag}^{-1}(\mathbf{r}_{t-1}) (2\overline{\mathbf{M}}\mathbf{f}_D - \overline{\mathbf{M}}_Q\mathbf{f}_Q)$
 $\nabla_{\mathbf{b}} L \leftarrow 2\Delta_{t-1} \text{diag}^{-1}(\mathbf{r}_{t-1}) (-2\mathbf{M}\mathbf{f}_D + \mathbf{M}_Q\mathbf{f}_Q)$
 update bounds: $\mathbf{a}_t \leftarrow \mathbf{a}_{t-1} - \eta \nabla_{\mathbf{a}} L$, $\mathbf{b}_t \leftarrow \mathbf{b}_{t-1} - \eta \nabla_{\mathbf{b}} L$
 $\mathbf{r}_t \leftarrow \mathbf{a}_t - \mathbf{b}_t$, update region volume Δ_t as in Eq (5)
end
Returns: robust region bounds: $\mathbf{a}_T, \mathbf{b}_T$.

Now, the loss and update directions are given as follows.

$$L(\mathbf{a}, \mathbf{b}) \approx \frac{(1 + \alpha)^n \mathbf{1}^T \mathbf{f}_Q}{\mathbf{1}^T \mathbf{f}_D} - 1$$

$$\nabla_{\mathbf{a}} L \approx \Delta (\text{diag}^{-1}(\mathbf{r}) \overline{\mathbf{M}}_D \mathbf{f}_D + \beta \text{diag}(\overline{\mathbf{M}} \mathbf{G}_D) + \beta \overline{\mathbf{s}})$$

$$\nabla_{\mathbf{b}} L \approx \Delta (-\text{diag}^{-1}(\mathbf{r}) \mathbf{M}_D \mathbf{f}_D + \beta \text{diag}(\mathbf{M} \mathbf{G}_D) + \beta \mathbf{s})$$
(16)

where the mask is the special mask

$$\overline{\mathbf{M}}_D = (\gamma_n \overline{\mathbf{M}} - \beta \mathbf{M}) ; \mathbf{M}_D = (\gamma_n \mathbf{M} - \beta \overline{\mathbf{M}}) ; \gamma_n = 2 - \beta(2n - 1)$$
(17)

\mathbf{s} is a weighted sum of the gradient from other dimensions ($i \neq k$) contributing to the update direction of dimension k , where $k \in \{1, 2, \dots, n\}$.

$$\mathbf{s}_k = \frac{1}{\mathbf{r}_k} \sum_{i=1, i \neq k}^n \mathbf{r}_i ((\overline{\mathbf{M}}_{i,:} - \mathbf{M}_{i,:}) \odot \overline{\mathbf{M}}_{k,:}) \mathbf{G}_{:,i}$$

$$\overline{\mathbf{s}}_k = \frac{1}{\mathbf{r}_k} \sum_{i=1, i \neq k}^n \mathbf{r}_i ((\mathbf{M}_{i,:} - \overline{\mathbf{M}}_{i,:}) \odot \mathbf{M}_{k,:}) \mathbf{G}_{:,i}$$
(18)

Algorithms 1, and 2 summarize the techniques explained above, which we implement in Section 4. The derivation of the 2-dimensional case and n -dimensional case of the OIR formulation, as well as other unsuccessful formulations are all included in the **supplement**.

4 Experiments

4.1 Setup and Data

In this paper, we chose the semantic parameters \mathbf{u} to be the azimuth rotations of the viewpoint and the elevation angle from the horizontal plane, where the

Algorithm 2: Robust n -dimensional Region Finding for White-Box DNNs by Outer-Inner Ratios

Requires: Semantic Function of a DNN $f(\mathbf{u})$ in Eq (1), initial semantic parameter \mathbf{u}_0 , learning rate η , object shape \mathbf{S}_z of class label z , emphasis factor β , Small ϵ

Form constant binary matrices $\mathbf{M}, \overline{\mathbf{M}}, \mathbf{M}_{\mathbb{D}}, \overline{\mathbf{M}}_{\mathbb{D}}$

Initialize bounds $\mathbf{a}_0 \leftarrow \mathbf{u}_0 - \epsilon \mathbf{1}$, $\mathbf{b}_0 \leftarrow \mathbf{u}_0 + \epsilon \mathbf{1}$

$\mathbf{r}_0 \leftarrow \mathbf{a}_0 - \mathbf{b}_0$, update region volume Δ_0 as in as in Eq (5)

for $t \leftarrow 1$ **to** T **do**

 form the all-corners function vector $f_{\mathbb{D}}$ as in Eq (7)

 form the all-corners gradients matrix $\mathbf{G}_{\mathbb{D}}$ as in Eq (15)

 form the gradient selection vectors $\mathbf{s}, \overline{\mathbf{s}}$ as in Eq (18)

$\nabla_{\mathbf{a}} L \leftarrow \Delta_{t-1} (\text{diag}^{-1}(\mathbf{r}_{t-1}) \overline{\mathbf{M}}_{\mathbb{D}} \mathbf{f}_{\mathbb{D}} + \beta \text{diag}(\overline{\mathbf{M}} \mathbf{G}_{\mathbb{D}} + \beta \overline{\mathbf{s}}))$

$\nabla_{\mathbf{b}} L \leftarrow \Delta_{t-1} (-\text{diag}^{-1}(\mathbf{r}_{t-1}) \mathbf{M}_{\mathbb{D}} \mathbf{f}_{\mathbb{D}} + \beta \text{diag}(\mathbf{M} \mathbf{G}_{\mathbb{D}}) + \beta \mathbf{s})$

 update bounds: $\mathbf{a}_t \leftarrow \mathbf{a}_{t-1} - \eta \nabla_{\mathbf{a}} L$, $\mathbf{b}_t \leftarrow \mathbf{b}_{t-1} - \eta \nabla_{\mathbf{b}} L$

$\mathbf{r}_t \leftarrow \mathbf{a}_t - \mathbf{b}_t$, update region volume Δ_t as in Eq (5)

end

Returns: robust region bounds: $\mathbf{a}_T, \mathbf{b}_T$.

object is always at the center of the rendering. This is common practise in the literature [17,20]. We use 100 shapes from 10 different classes from ShapeNet [7], the largest dataset for 3D models that are normalized from the semantic lens. We pick these 100 shapes specifically such that: (1) the class label is available in ImageNet [32] and that ImageNet classifiers can identify the exact class, and (2) the selected shapes are identified by the classifiers at some part of the semantic space. To do this, we measured the average score in the space and accepted the shape only if its average Resnet softmax score is 0.1. To render the images, we use a differentiable renderer NMR [22], which allows obtaining the gradient to the semantic input parameters. The networks of interest are Resnet50 [19], VGG [35], AlexNet [23], and InceptionV3 [37]. We use the official PyTorch implementation for each network [30].

4.2 Mapping the Networks

Similar to Fig. 1, we map the networks for all 100 shapes on the first semantic parameter (the azimuth rotation), as well as the joint (azimuth and elevation). We show these results in Fig. 4. The ranges for the two parameters were $[0^\circ, 360^\circ], [-10^\circ, 90^\circ]$, with a 3×3 grid. The total number of network evaluations is 4K forward passes from each network for every shape (total of 1.6M forward passes). We show all of the remaining results in the **supplement**.

4.3 Growing Semantic Robust Regions

We implement the three bottom-up approaches in Table 2 and Algorithms 1 and 2. The hyper-parameters were set to $\eta = 0.1, \alpha = 0.05, \beta = 0.0009, \lambda = 0.1, T = 800$.

Deep Networks	SRVR	Top-1 error	Top-5 Error
AlexNet [23]	8.87%	43.45	20.91
VGG-11 [35]	9.72%	30.98	11.37
ResNet50 [19]	16.79%	23.85	7.13
Inceptionv3 [37]	7.92%	22.55	6.44

Table 1: **Benchmarking popular DNNs in Semantic Robustness vs error rate.** We develop the Semantic Robustness Volume Ratio (SRVR) metric to quantify and compare the semantic robustness of well-known DNNs in Section 4.4. We see that semantic robustness does not necessarily depend on the accuracy of the DNN. This motivates studying it as an independent metric from the classification accuracy. Results are reported based on the official PyTorch implementations of these networks [30].

Analysis Approach	Paradigm	Total Sampling complexity	Black-box Functions	Forward pass /step	Backward pass /step	Identification Capability
Grid Sampling	top-down	$\mathcal{O}(N^n)$ $N \gg 2$	✓	-	-	Fully identifies the semantic map of DNN
Naive	bottom-up	$\mathcal{O}(2^n)$	✓	2^n	0	finds strong robust regions only around \mathbf{u}_0
OIR_B	bottom-up	$\mathcal{O}(2^{n+1})$	✓	2^{n+1}	0	finds strong and weak robust regions around \mathbf{u}_0
OIR_W	bottom-up	$\mathcal{O}(2^n)$	✗	2^n	2^n	finds strong and weak robust regions around \mathbf{u}_0

Table 2: **Semantic Analysis Techniques:** We compare different approaches to analyse the semantic robustness of DNNs.

We can observe in Fig. 3 that multiple initial points inside the same robust region converge to the same boundary. One key difference to be noted between the naive approach in Eq (8) and the OIR formulations in Eq (11,16) is that the naive approach fails to capture robust regions in some scenarios and fall for trivial regions (see Fig. 3).

4.4 Applications

Quantifying Semantic Robustness.

Looking at these NSM can lead to insights about the network, but we would like to develop a systemic approach to quantify the robustness of these DNNs. To do this, we develop the Semantic Robustness Volume Ratio (SRVR) metric. The SRVR of a network is the ratio between the expected size of the robust region obtained by Algorithms 1 and 2 over the nominal total volume of the semantic map of interest. Explicitly, the SRVR of network \mathbf{C} for class label z is defined as follows:

$$\text{SRVR}_z = \frac{\mathbb{E}[\text{Vol}(\mathbb{D})]}{\text{Vol}(\Omega)} = \frac{\mathbb{E}_{\mathbf{u}_0 \sim \Omega, \mathbf{S}_z \sim \mathbb{S}_z}[\text{Vol}(\Phi(f, \mathbf{S}_z, \mathbf{u}_0))]}{\text{Vol}(\Omega)}, \quad (19)$$

Average confidence score of CUP class in ImageNet

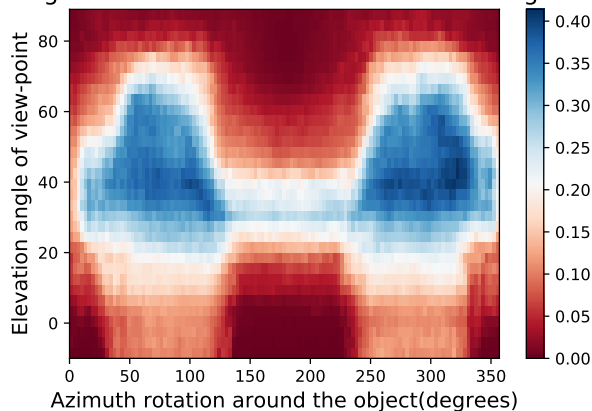


Fig. 5: **Semantic Bias in ImageNet.** By taking the average semantic maps over 10 shapes of *cup* class and over different networks, we can visualize the bias of the training data. The angles of low score are probably not well-represented in ImageNet [32].

where f, Φ are defined in Eq (1,2) respectively. We take the average volume of all the adversarial regions found for multiple initializations and multiple shapes of the same class z . Then, we divide by the volume of the entire space. This provides a percentage of how close the DNN is from the ideal behaviour of identifying the object robustly in the entire space. The SRVR metric is not strict in its value, since the analyzer defines the semantic space of interest and the shapes used. However, comparing SRVR scores among DNNs is of extreme importance, as this relative analysis conveys insights about a network that might not be evident by only observing the accuracy of this network. For example, we can see in Table 1 that while InceptionV3 [37] is the best in terms of accuracy, it lags behind Resnet50 [19] in terms of semantic robustness. This observation is also consistent with the qualitative NSMs in Fig. 4, in which we can see that while Inception is very confident, it can fail completely inside these confident regions. Note that the reported SRVR results are averaged over all 10 classes and over all 100 shapes. We use 4 constant initial points for all experiments and the semantic parameters are the azimuth and elevation as in Fig. 3 and 4. As can be seen in Fig. 3, different methods predict different regions, so we take the average size of the the three methods used (naive, OIR_W, and OIR_B) to give an overall estimate of the volume used in the SRVR results reported in Table 1.

Finding Semantic Bias in the Data.

While observing the above figures uncovers interesting insights about the DNNs and the training data of ImageNet [32], it does not allow to make a conclusion about the network nor about the data. Therefore, we can average these semantic maps of these networks to factor out the effect of the network structure and training and maintain only the effect of training data. We show two such maps

called Data Semantic Maps (DSMs). We observe that networks have holes in their semantic maps and these holes are shared among DNNs, indicating bias in the data. Identifying this gap in the data can help train a more semantically robust network. This can be done by leveraging adversarial training on these data-based adversarial regions as performed in the adversarial attack literature [15]. Fig. 5 shows an example of this semantic map, which points to the possibility that ImageNet [32] may not contain angles of the easy *cup* class.

5 Analysis

First, we observe in Fig. 4 that some red areas (adversarial regions the DNN can not identify the object within) are surrounded by blue areas (robust regions the DNN can identify the object within). These “semantic traps” are dangerous in ML, since they are hard to identify (without NSM) and they can cause failure cases for some models. These traps can be attributed to either the model architecture, training, and loss, or bias in the dataset, on which the model was trained (*i.e.* ImageNet [32]).

Note that plotting NMS is extremely expensive even for a moderate dimensionality *e.g.* $n = 8$. For example, for the plot in Fig. 1, we use $N = 180$ points in the range of 360 degrees. If all the other dimensions require the same number of samples for their individual range, the total joint space requires $180^n = 180^8 = 1.1 \times 10^{18}$ samples, which is enormous. Evaluating the DNN for that many forward passes is intractable. Thus, we follow a bottom-up approach instead, where we start from one point in the semantic space \mathbf{u}_0 and we grow an n -dimensional hyper-rectangle around that point to find the robust “neighborhood” of that point for this specific DNN. Table 2 compares different analysis approaches for semantic robustness of DNNs.

6 Conclusion

We analyse DNN robustness with a semantic lens and show how more confident networks tend to create adversarial semantic regions inside highly confident regions. We developed a bottom-up approach to semantically analyse networks by growing adversarial regions. This approach scales well with dimensionality, and we use it to benchmark the semantic robustness of several well-known and popular DNNs.

Acknowledgments. This work was supported by the King Abdullah University of Science and Technology (KAUST) Office of Sponsored Research under Award No. OSR-CRG2018-3730

References

1. Alcorn, M.A., Li, Q., Gong, Z., Wang, C., Mai, L., Ku, W.S., Nguyen, A.: Strike (with) a pose: Neural networks are easily fooled by strange poses of familiar objects. In: The IEEE Conference on Computer Vision and Pattern Recognition (CVPR) (June 2019)
2. An, G.: The effects of adding noise during backpropagation training on a generalization performance. *Neural computation* **8**(3), 643–674 (1996)
3. Bibi, A., Alfadly, M., Ghanem, B.: Analytic expressions for probabilistic moments of pl-dnn with gaussian input. In: The IEEE Conference on Computer Vision and Pattern Recognition (CVPR) (June 2018)
4. Bishop, C.M.: Training with noise is equivalent to tikhonov regularization. *Training* **7**(1) (2008)
5. Boyd, S., Vandenberghe, L.: *Convex Optimization*. Cambridge University Press, New York, NY, USA (2004)
6. Carlini, N., Wagner, D.: Towards evaluating the robustness of neural networks. In: IEEE Symposium on Security and Privacy (SP) (2017)
7. Chang, A.X., Funkhouser, T., Guibas, L., Hanrahan, P., Huang, Q., Li, Z., Savarese, S., Savva, M., Song, S., Su, H., Xiao, J., Yi, L., Yu, F.: ShapeNet: An Information-Rich 3D Model Repository. Tech. Rep. arXiv:1512.03012 [cs.GR], Stanford University — Princeton University — Toyota Technological Institute at Chicago (2015)
8. Chen, P.Y., Zhang, H., Sharma, Y., Yi, J., Hsieh, C.J.: Zoo: Zeroth order optimization based black-box attacks to deep neural networks without training substitute models. In: Proceedings of the 10th ACM Workshop on Artificial Intelligence and Security. pp. 15–26. AISeC '17, ACM, New York, NY, USA (2017)
9. Dosovitskiy, A., Brox, T.: Inverting visual representations with convolutional networks. In: Proceedings of the IEEE Conference on Computer Vision and Pattern Recognition. pp. 4829–4837 (2016)
10. Dreossi, T., Jha, S., Seshia, S.A.: Semantic adversarial deep learning. In: International Conference on Computer Aided Verification. pp. 3–26. Springer (2018)
11. Engstrom, L., Tran, B., Tsipras, D., Schmidt, L., Madry, A.: Exploring the landscape of spatial robustness. In: Proceedings of the 36th International Conference on Machine Learning (ICML) (2019)
12. Fawzi, A., Moosavi-Dezfooli, S.M., Frossard, P.: Robustness of classifiers: from adversarial to random noise. In: Advances in Neural Information Processing Systems (2016)
13. Fawzi, A., Moosavi Dezfooli, S.M., Frossard, P.: The robustness of deep networks - a geometric perspective. *IEEE Signal Processing Magazine* (2017)
14. Geirhos, R., Rubisch, P., Michaelis, C., Bethge, M., Wichmann, F.A., Brendel, W.: Imagenet-trained cnns are biased towards texture; increasing shape bias improves accuracy and robustness. arXiv preprint arXiv:1811.12231 (2018)
15. Goodfellow, I., Shlens, J., Szegedy, C.: Explaining and harnessing adversarial examples. In: International Conference on Learning Representations (ICLR) (2015)
16. Grandvalet, Y., Canu, S., Boucheron, S.: Noise injection: Theoretical prospects. *Neural Computation* **9**(5), 1093–1108 (1997)
17. Hamdi, A., Muller, M., Ghanem, B.: SADA: semantic adversarial diagnostic attacks for autonomous applications. In: AAAI Conference on Artificial Intelligence (2020)
18. Hamdi, A., Rojas, S., Thabet, A., Ghanem, B.: Advpc: Transferable adversarial perturbations on 3d point clouds (2019)
19. He, K., Zhang, X., Ren, S., Sun, J.: Deep residual learning for image recognition. *CoRR* **abs/1512.03385** (2015)

20. Hosseini, H., Poovendran, R.: Semantic adversarial examples. CoRR **abs/1804.00499** (2018)
21. Kato, H., Ushiku, Y., Harada, T.: Neural 3d mesh renderer. In: The IEEE Conference on Computer Vision and Pattern Recognition (CVPR) (June 2018)
22. Kato, H., Ushiku, Y., Harada, T.: Neural 3d mesh renderer. In: Proceedings of the IEEE Conference on Computer Vision and Pattern Recognition. pp. 3907–3916 (2018)
23. Krizhevsky, A., Sutskever, I., Hinton, G.E.: Imagenet classification with deep convolutional neural networks. In: Pereira, F., Burges, C.J.C., Bottou, L., Weinberger, K.Q. (eds.) Advances in Neural Information Processing Systems 25, pp. 1097–1105. Curran Associates, Inc. (2012)
24. Kurakin, A., Goodfellow, I.J., Bengio, S.: Adversarial machine learning at scale. CoRR **abs/1611.01236** (2016)
25. Liu, H.T.D., Tao, M., Li, C.L., Nowrouzezahrai, D., Jacobson, A.: Beyond pixel norm-balls: Parametric adversaries using an analytically differentiable renderer. In: International Conference on Learning Representations (2019)
26. Mahendran, A., Vedaldi, A.: Understanding deep image representations by inverting them. CoRR **abs/1412.0035** (2014)
27. Moosavi-Dezfooli, S.M., Fawzi, A., Fawzi, O., Frossard, P.: Universal adversarial perturbations. In: The IEEE Conference on Computer Vision and Pattern Recognition (CVPR) (2017)
28. Moosavi-Dezfooli, S.M., Fawzi, A., Frossard, P.: Deepfool: A simple and accurate method to fool deep neural networks. In: The IEEE Conference on Computer Vision and Pattern Recognition (CVPR) (June 2016)
29. Nitin Bhagoji, A., He, W., Li, B., Song, D.: Practical black-box attacks on deep neural networks using efficient query mechanisms. In: The European Conference on Computer Vision (ECCV) (September 2018)
30. Paszke, A., Gross, S., Chintala, S., Chanan, G., Yang, E., DeVito, Z., Lin, Z., Desmaison, A., Antiga, L., Lerer, A.: Automatic differentiation in pytorch. In: NIPS-W (2017)
31. Ródenas, R.G., López, M.L., Verastegui, D.: Extensions of dinkelbach’s algorithm for solving non-linear fractional programming problems. Top **7**(1), 33–70 (Jun 1999)
32. Russakovsky, O., Deng, J., Su, H., Krause, J., Satheesh, S., Ma, S., Huang, Z., Karpathy, A., Khosla, A., Bernstein, M.S., Berg, A.C., Li, F.: Imagenet large scale visual recognition challenge. CoRR **abs/1409.0575** (2014)
33. Shou, Z., Gao, H., Zhang, L., Miyazawa, K., Chang, S.F.: Autoloc: weakly-supervised temporal action localization in untrimmed videos. In: Proceedings of the European Conference on Computer Vision (ECCV). pp. 154–171 (2018)
34. Shu, M., Liu, C., Qiu, W., Yuille, A.: Identifying model weakness with adversarial examiner. Proceedings of the AAAI Conference on Artificial Intelligence **34**(07), 11998–12006 (Apr 2020)
35. Simonyan, K., Zisserman, A.: Very deep convolutional networks for large-scale image recognition. arXiv preprint arXiv:1409.1556 (2014)
36. Stroud, A.H.: Methods of numerical integration (philip j. davis and philip rabinowitz). SIAM Review **18**(3), 528–2 (07 1976)
37. Szegedy, C., Vanhoucke, V., Ioffe, S., Shlens, J., Wojna, Z.: Rethinking the inception architecture for computer vision. In: Proceedings of the IEEE conference on computer vision and pattern recognition. pp. 2818–2826 (2016)
38. Szegedy, C., Zaremba, W., Sutskever, I., Bruna, J., Erhan, D., Goodfellow, I., Fergus, R.: Intriguing properties of neural networks. ICLR (2013)
39. Szegedy, C., Zaremba, W., Sutskever, I., Bruna, J., Erhan, D., Goodfellow, I.J., Fergus, R.: Intriguing properties of neural networks. CoRR **abs/1312.6199** (2013)

40. Torralba, A., Efros, A.A.: Unbiased look at dataset bias. In: CVPR (2011)
41. Vondrick, C., Khosla, A., Malisiewicz, T., Torralba, A.: Hoggles: Visualizing object detection features. In: Proceedings of the IEEE International Conference on Computer Vision. pp. 1–8 (2013)
42. Zeng, X., Liu, C., Wang, Y.S., Qiu, W., Xie, L., Tai, Y.W., Tang, C.K., Yuille, A.L.: Adversarial attacks beyond the image space. In: The IEEE Conference on Computer Vision and Pattern Recognition (CVPR) (June 2019)

A Analyzing Deep Neural Networks

Here we visualize different Network semantic maps generated during our analysis. In the 1D case we fix the elevation of the camera to a nominal angle of 35° and rotate around the object. In the 2D case, we change both the elevation and azimuth around the object. These maps can be generated to any type of semantic parameters that affect the generation of the image, and not viewing angle.

A.1 Networks Semantic Maps (1D)

In Fig. 6,7 we visualize the 1D semantic maps of rotating around the object and recording different DNNs performance and averaging the profile over 10 different shapes per class.

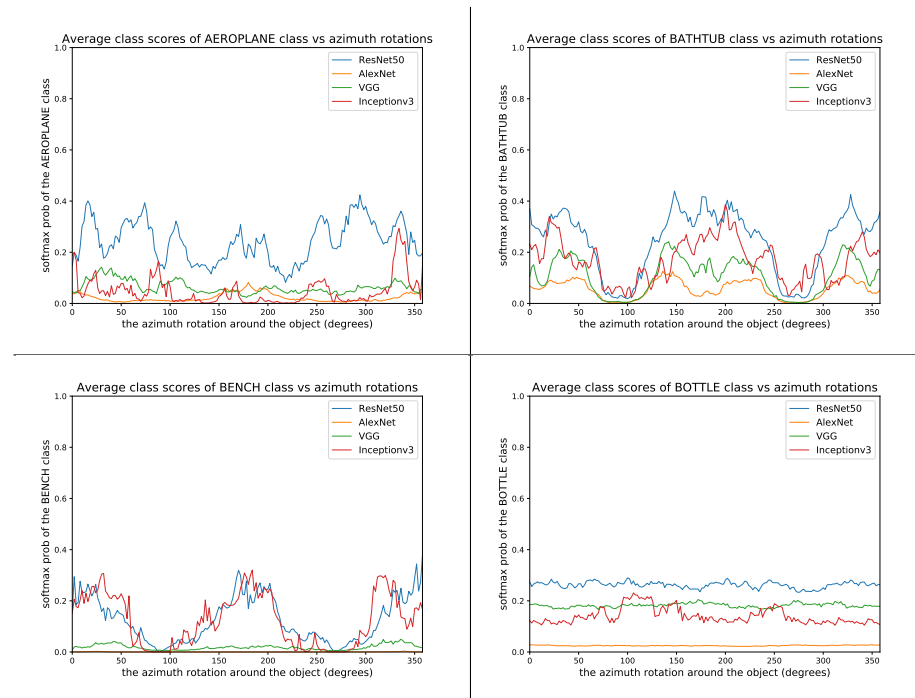


Fig. 6: **1D Network Semantic Maps NMS-I**: visualizing 1D Semantic Robustness profile for different networks averaged over 10 different shapes. Observe that different DNNs profiles differ depending on the training, accuracy, and network architectures that all result in a unique "signatures" for the DNN on that class. The correlation between the DNN profiles is due to the common data bias in ImageNet.

A.2 Networks Semantic Maps (2D)

In Fig. 8,9 we visualize the 2D semantic maps of elevation angles and rotating around the object and recording different DNNs performance and averaging the maps over 10 different shapes per class.

A.3 Convergence of the Region Finding Algorithms

Here we show how when we apply the region detection algorithms; the naive detect the smallest region while the OIR formulations detect bigger more general robust region. This result happens even with different initial points; they always converge to the same bounds of that robust region of the semantic maps. Fig. 10 show 4 different initializations for 1D case along with predicted regions. In Fig. 11,12 shows the bounds evolving during the optimization of the three algorithms (naive , OIR_B and OIR_W) for 500 steps.

A.4 Examples of Found Regions (with Example Renderings)

In Fig. 13,14 we provide examples of 2D regions found with the three algorithms along with renderings of the shapes from the robust regions detected.

A.5 Analyzing Semantic Data Bias in ImageNet

In Fig. 15,16, we visualizing semantic data bias in the common training dataset (*i.e.* ImageNet [32]) by averaging the Networks Semantic Maps (NSM) of different networks and on different shapes, Different classes have a different semantic bias in ImageNet as clearly shown in the maps above. These places of high confidence probably reveal the areas where an abundance of examples exists in ImageNet, while holes convey scarcity of such examples in ImageNet corresponding class.

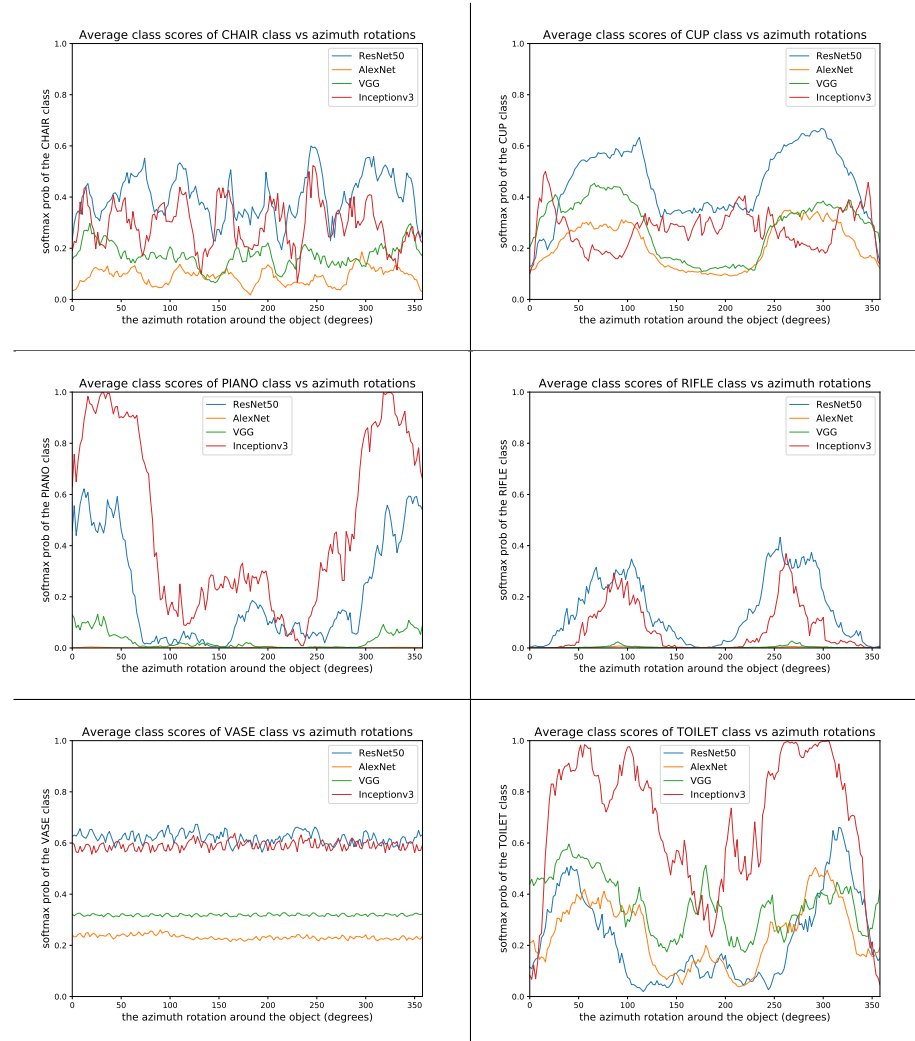


Fig. 7: **1D Network Semantic Maps NMS-II**: visualizing 1D Semantic Robustness profile for different networks averaged over 10 different shapes. Observe that different DNNs profiles differ depending on the training , accuracy , and network architectures that all result in a unique "signatures" for the DNN on that class. The correlation between the DNN profiles is due to the common data bias in ImageNet.

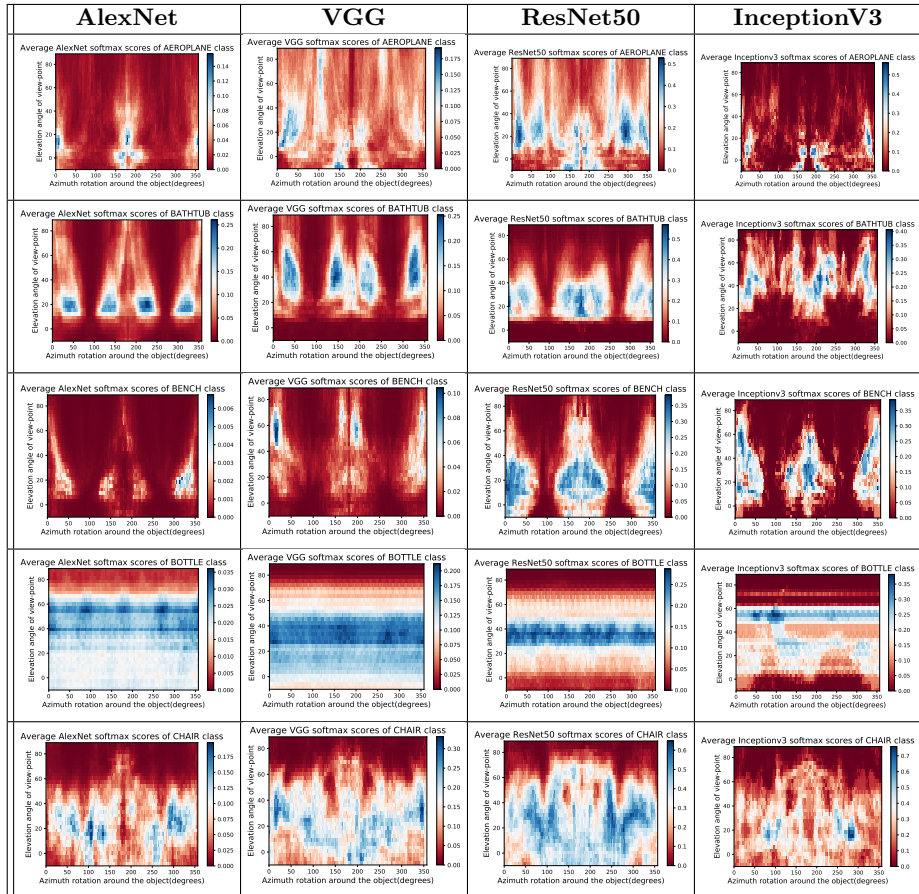


Fig. 8: 2D Network Semantic Maps NMS-I. Visualizing 2D Semantic Robustness profile for different networks averaged over 10 different shapes. Every row is different class. observe that different DNNs profiles differ depending on the training , accuracy , and network architectures that all result in a unique "signatures" for the DNN on that class.

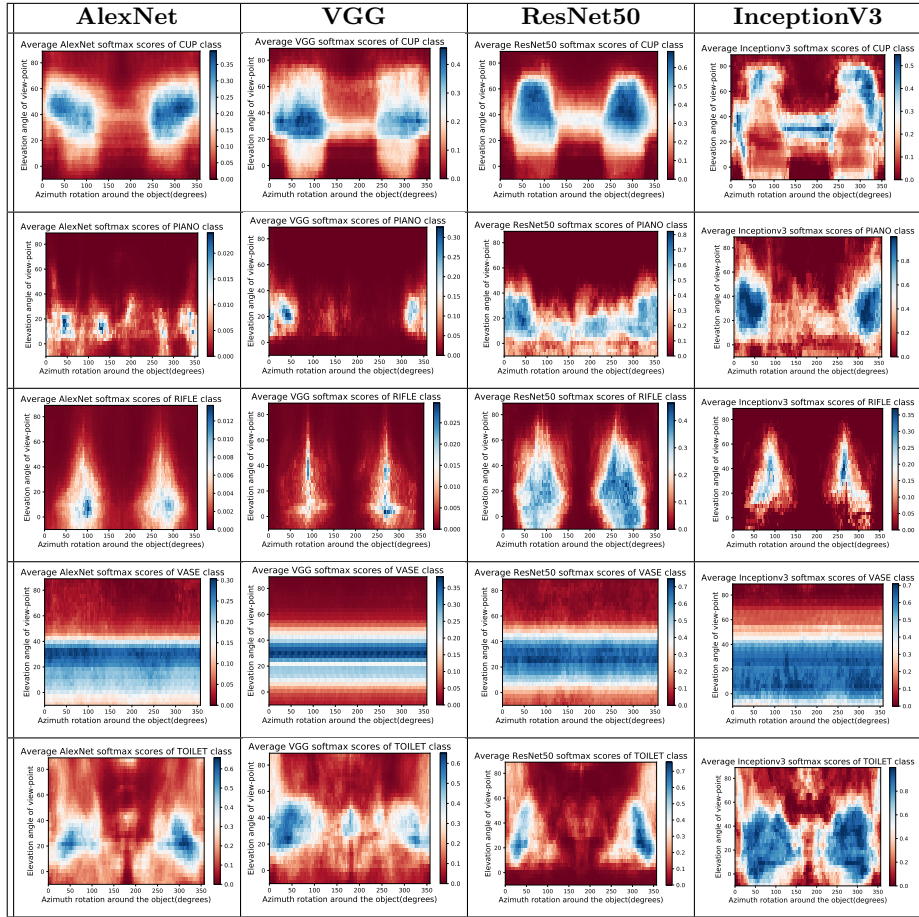


Fig. 9: **2D Network Semantic Maps NMS-II**: visualizing 2D Semantic Robustness profile for different networks averaged over 10 different shapes. Every row is different class. observe that different DNNs profiles differ depending on the training , accuracy , and network architectures that all result in a unique "signatures" for the DNN on that class.

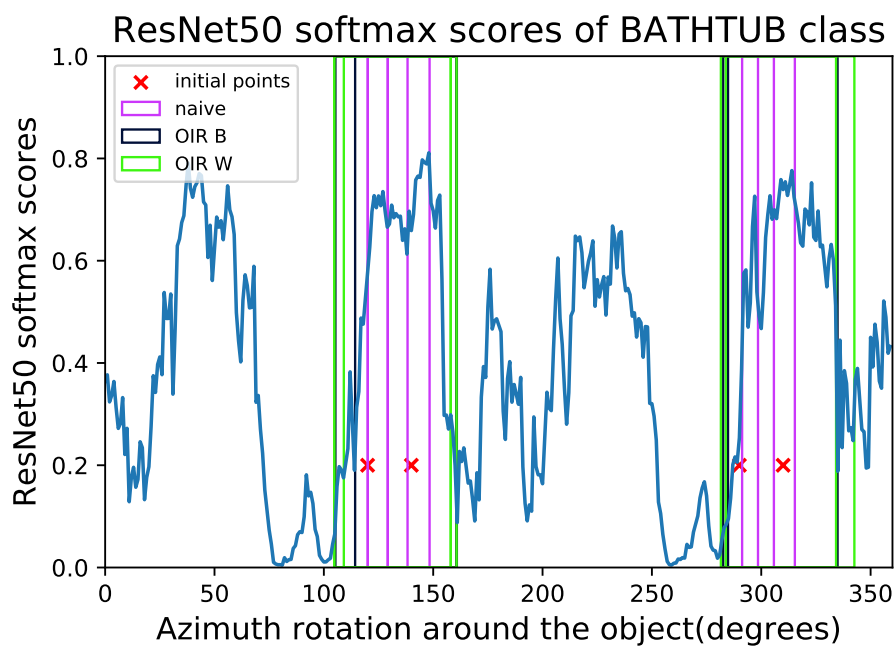


Fig. 10: **Robust Region Detection with different initializations:** visualizing the Robust Regions Bounds found by the three algorithms for four initial points. We can see that the naive produce different bounds of the same region for different initializations while OIR detect the same region regardless of initialization.

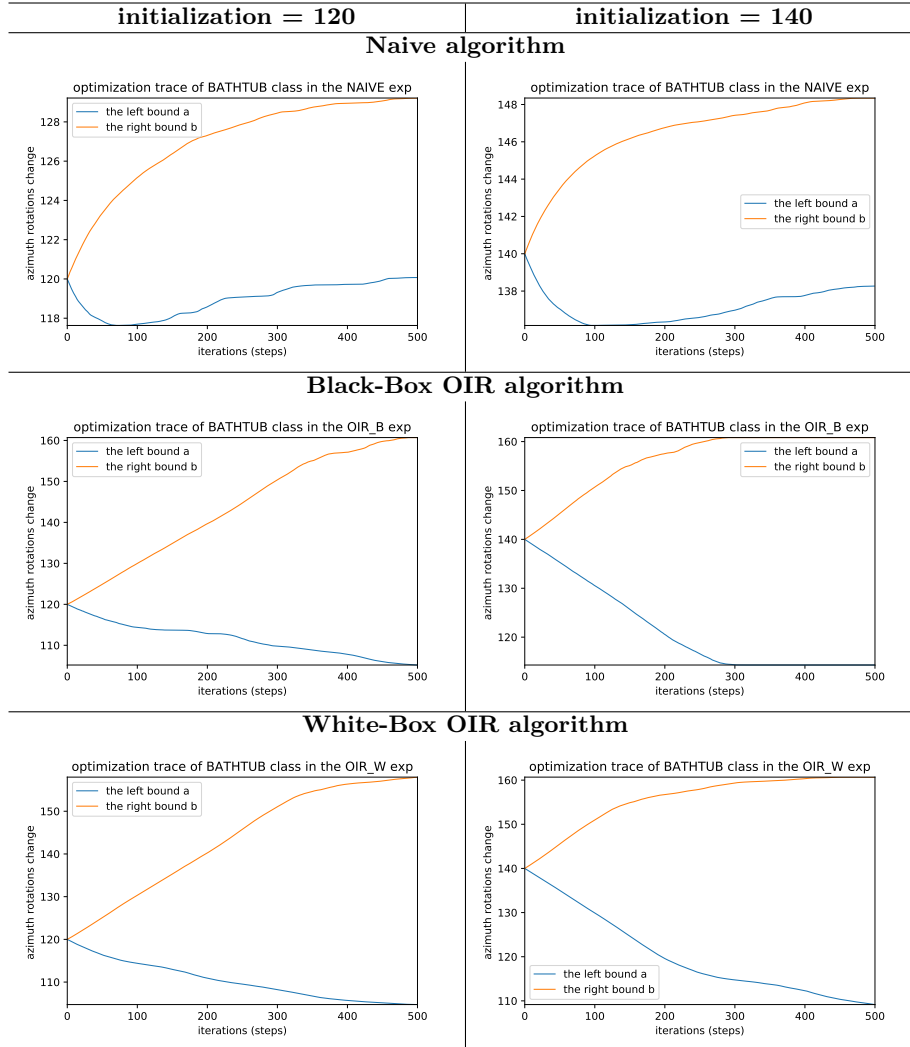


Fig. 11: Robust Region Bounds Growing I: visualizing the bounds growing Using different algorithms from two different initializations (120 and 140) in Fig. 10. We can see that OIR formulations converge to the same bounds of the robust region regardless of the initialization, which indicates effectiveness in detecting these regions, unlike the naive approach which can stop in a local optimum.

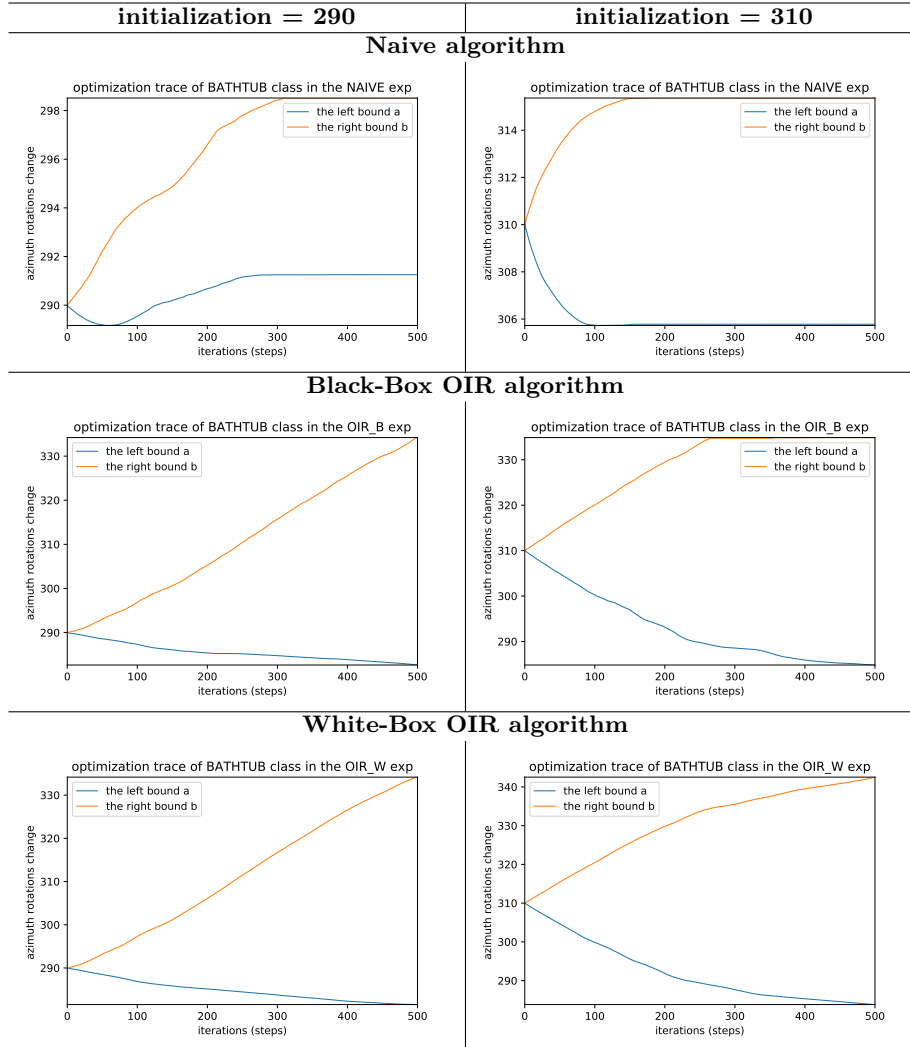


Fig. 12: **Robust Region Bounds Growing I**: visualizing the bounds growing Using different algorithms from two different initializations (290, 310) in Fig. 10. We can see that OIR formulations converge to the same bounds of the robust region regardless of the initialization, which indicates effectiveness in detecting these regions, unlike the naive approach which can stop in a local optimum.

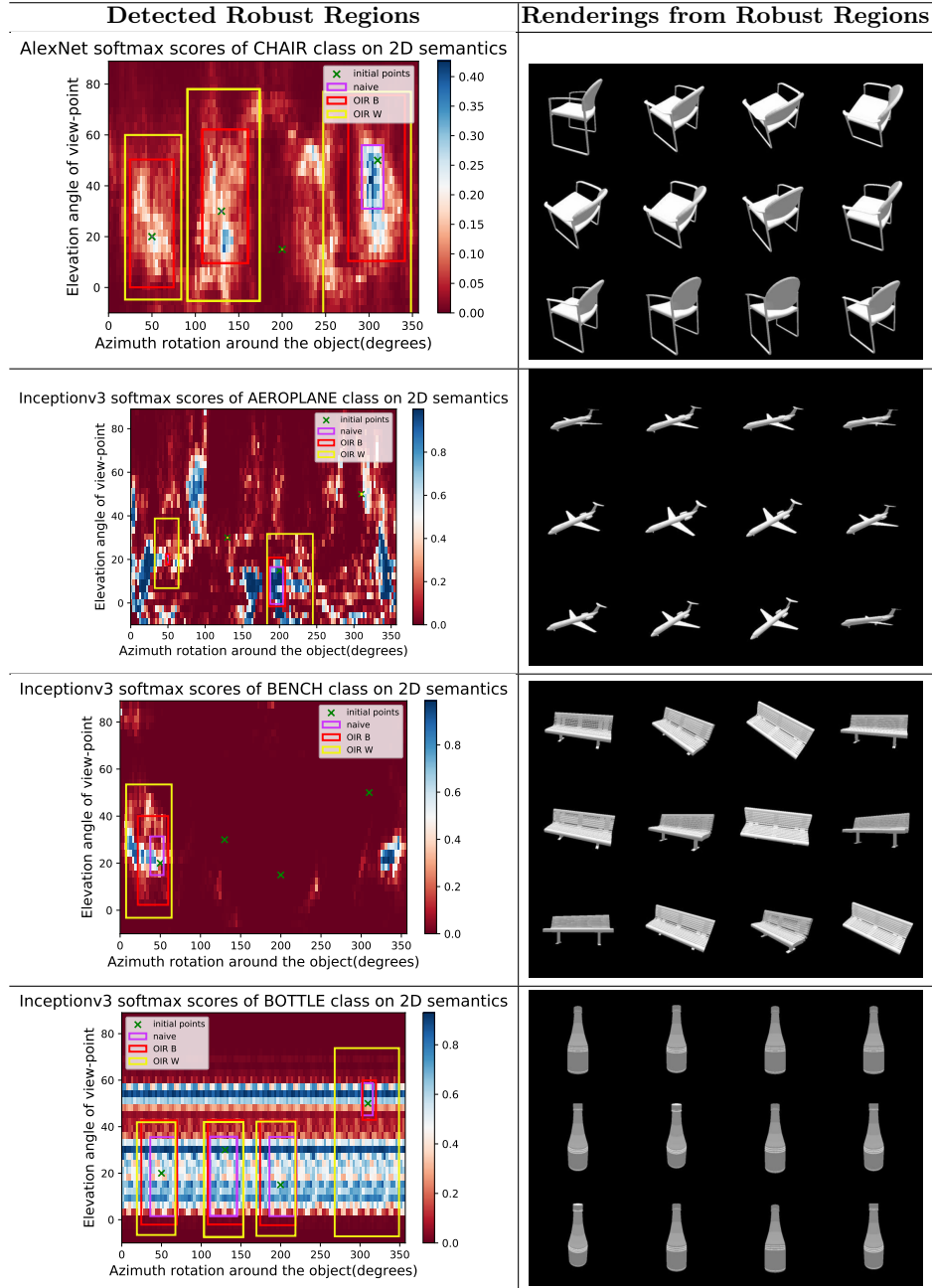


Fig. 13: **Qualitative Examples of Robust Regions I:** visualizing different runs of the algorithm to find robust regions along with different renderings from inside these regions for those specific shapes used in the experiments.

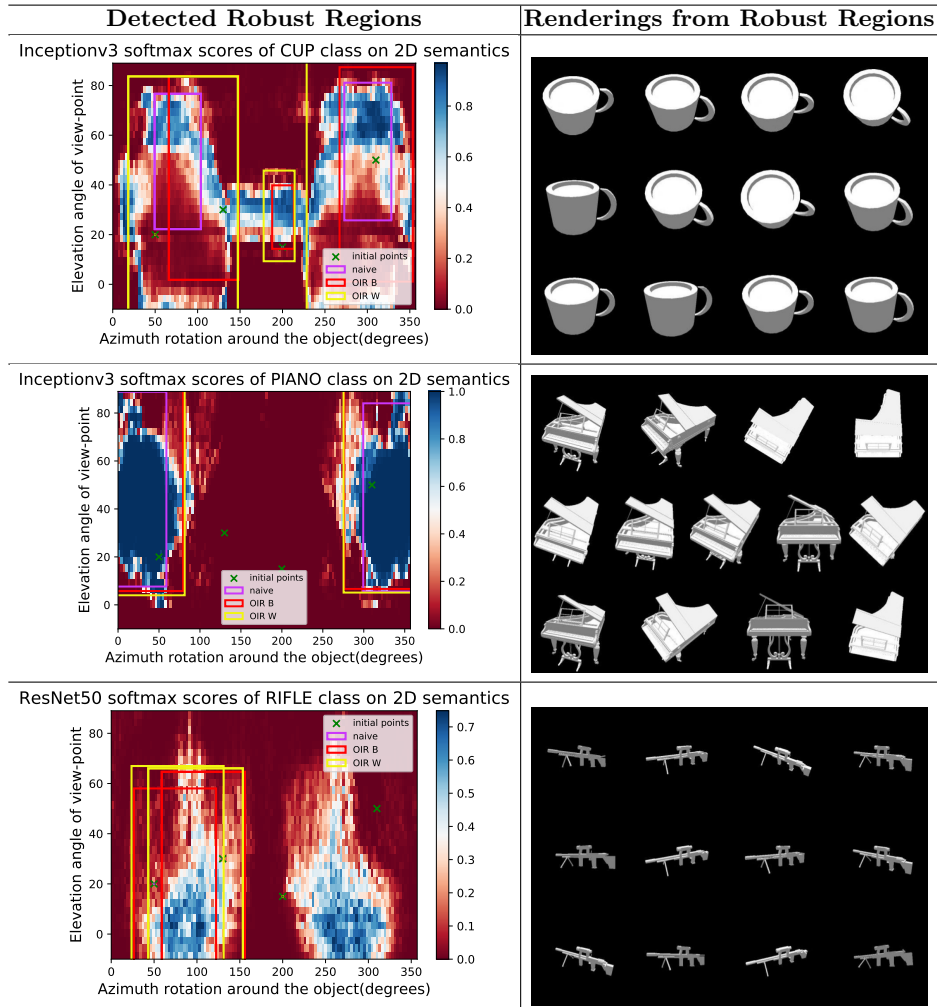


Fig. 14: **Qualitative Examples of Robust Regions II**: visualizing different runs of the algorithm to find robust regions along with different renderings from inside these regions for those specific shapes used in the experiments.

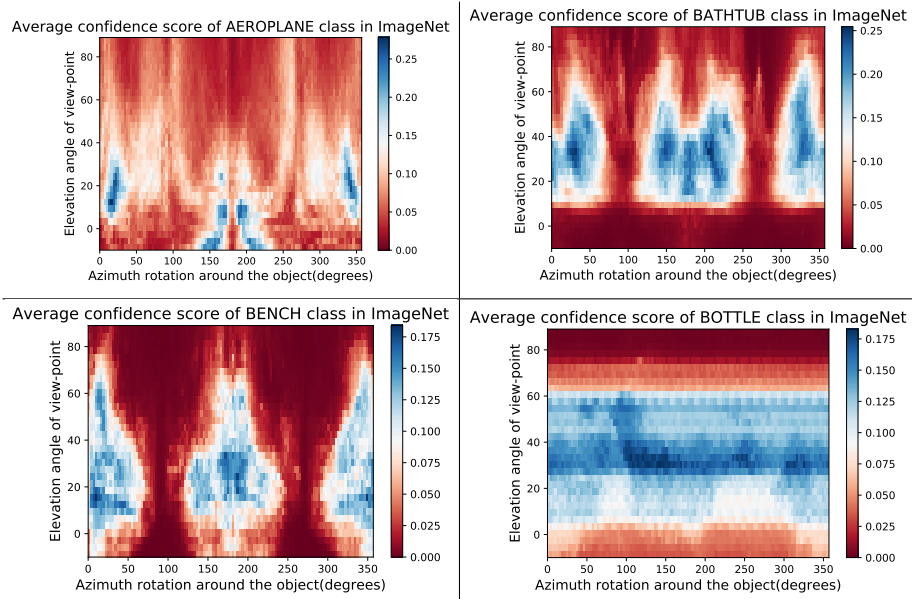


Fig. 15: **Data Semantic Maps DSM-I**: visualizing Semantic Data Bias in the common training dataset (*i.e.* ImageNet [32]) by averaging the Networks Semantic Maps (NSM) of different networks and on different shapes, Different classes have different semantic bias in ImageNet as clearly shown in the maps above. The symmetry in the maps are attributed to the 3D symmetry of the objects.

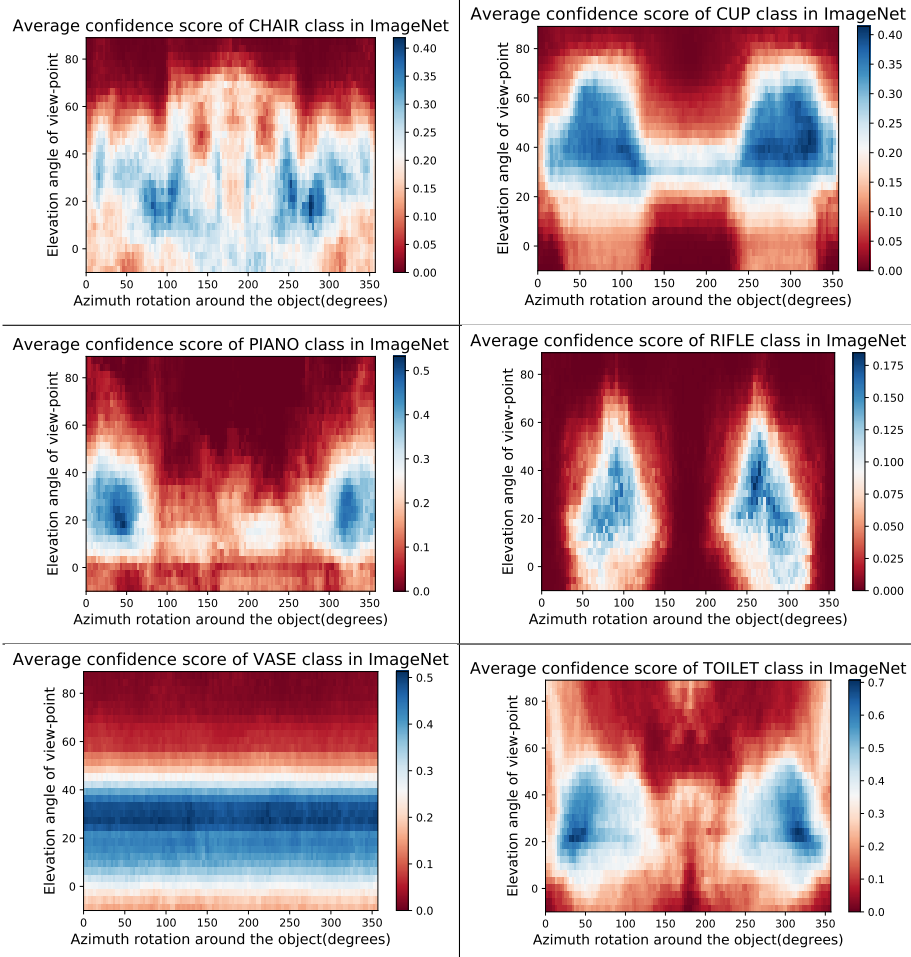


Fig. 16: **Data Semantic Maps DSM-II:** visualizing Semantic Data Bias in the common training dataset (*i.e.* ImageNet [32]) By averaging the Networks Semantic Maps (NSM) of different networks and on different shapes, Different classes have different semantic bias in ImageNet as clearly shown in the maps above. The symmetry in the maps are attributed to the 3D symmetry of the objects.

B Detailed Derivations of the Update Directions of the Bounds

B.1 Defining Robustness as an Operator

In our case we consider a more general case where we are interested in the $\mathbf{u} \in \Omega \subset \mathbb{R}^n$, a hidden latent parameter that generates the image and is passed to a scene generator (e.g. a renderer function \mathbf{R}) that takes the parameter \mathbf{u} and an object shape \mathbf{S} of a class that is identified by classifier \mathbf{C} . Ω is the continuous semantic space for the parameters that we intend to study. The renderer creates the image $\mathbf{x} \in \mathbb{R}^d$, and then we study the behavior of a classifier \mathbf{C} of that image across multiple shapes and multiple famous DNNs. Now, this function of interest is defined as follows.

$$f(\mathbf{u}) = \mathbf{C}_z(\mathbf{R}(\mathbf{S}_z, \mathbf{u})), \quad 0 \leq f(\mathbf{u}) \leq 1 \quad (20)$$

Where z is a class label of interest of study, and we observe the network score for that class by rendering a shape \mathbf{S}_z of the same class. The shape and class labels are constants, and only the parameters vary for f . The robust-region-finding operator is then defined as follows

$$\begin{aligned} \Phi_{\text{robust}}(f(\mathbf{u}), \mathbf{S}_z, \mathbf{u}_0) &= \mathbb{D} = \{\mathbf{u} : \mathbf{a} \leq \mathbf{u} \leq \mathbf{b}\} \\ \text{s.t. } \mathbb{E}_{\mathbf{u} \sim \mathbb{D}}[f(\mathbf{u})] &\geq 1 - \epsilon_m, \quad \mathbf{u}_0 \in \mathbb{D}, \quad \text{VAR}[f(\mathbf{u})] \leq \epsilon_v \end{aligned} \quad (21)$$

where the left and right bounds of \mathbb{D} are $\mathbf{a} = [a_1, a_2, \dots, a_n]$ and $\mathbf{b} = [b_1, b_2, \dots, b_n]$ respectively. The two small thresholds ϵ_m, ϵ_v are to insure high performance and low variance of the DNN network in that robust region. We can define the opposite operator which is to find adversarial regions like follows :

$$\begin{aligned} \Phi_{\text{adv}}(f(\mathbf{u}), \mathbf{S}_z, \mathbf{u}_0) &= \mathbb{D} = \{\mathbf{u} : \mathbf{a} \leq \mathbf{u} \leq \mathbf{b}\} \\ \text{s.t. } \mathbb{E}_{\mathbf{u} \sim \mathbb{D}}[f(\mathbf{u})] &\leq \epsilon_m, \quad \mathbf{u}_0 \in \mathbb{D}, \quad \text{VAR}[f(\mathbf{u})] \geq \epsilon_v \end{aligned} \quad (22)$$

We can show clearly that Φ_{adv} and Φ_{robust} are related as follows

$$\Phi_{\text{adv}}(f(\mathbf{u}), \mathbf{S}_z, \mathbf{u}_0) = \Phi_{\text{robust}}(1 - f(\mathbf{u}), \mathbf{S}_z, \mathbf{u}_0) \quad (23)$$

So we can just focus our attention on Φ_{robust} to find robust regions, and the adversarial regions follow directly from Eq (23).

B.2 Divergence of the Bounds

To develop an algorithm for Φ , we deploy the idea by [33] which focuses on maximizing the inner area of the function in the region and fitting the bounds to grow the region bounds. As we will show, maximizing the region by maximizing the integral can lead to divergence, as follows :

Lemma 1. *Let f be a continuous scalar function $f : \mathbb{R}^1 \rightarrow \mathbb{R}^1$, and let L be the function defining the definite integral of f in terms of the two integral bounds, i.e. $L(a, b) = \int_a^b f(u) du$. Then, to maximize L , $-f(a)$ and $f(b)$ are valid ascent directions for the two bounds a, b respectively.*

Proof. a direction \mathbf{p} is an ascent direction of objective L if it satisfies the inequality $\mathbf{p}^T \nabla L \geq 0$. [5].

To find $\frac{\partial L}{\partial a} = \frac{\partial}{\partial a} \int_a^b f(u) du$, we use Leibniz rule from the fundamental theorem of calculus which states that $\frac{d}{dx} \int_{a(x)}^{b(x)} f(u) du = f(b(x)) \frac{d}{dx} b(x) - f(a(x)) \frac{d}{dx} a(x)$

Therefore, $\frac{\partial}{\partial a} \int_a^b f(u) du = f(b) \times 0 - f(a) \times 1 = -f(a)$. Similarly, $\frac{\partial}{\partial b} \int_a^b f(u) du = f(b)$. By picking $\mathbf{p} = [-f(a), f(b)]^T$, then $\mathbf{p}^T \nabla L = f(a)^2 + f(b)^2 \geq 0$. This proves that \mathbf{p} is a valid ascent direction for objective L .

Theorem 1. *Let f be a positive continuous scalar function $f : \mathbb{R}^1 \rightarrow (0, 1)$, and let L be the function defining the definite integral of f in terms of the two integral bounds, i.e. $L(a, b) = \int_a^b f(u) du$. Then, following the ascent direction in Lemma 1 can diverge the bounds if followed in a gradient ascent technique with fixed learning rate.*

Proof. If we follow the direction $[-f(a), f(b)]^T$, with a fixed learning rate η , then the update rules for a, b will be as follows. $a_k = a_{k-1} - \eta f(a)$, $b_k = b_{k-1} + \eta f(b)$. for initial points a_0, b_0 , then $a_k = a_0 - \eta \sum_{i=0}^k f(a_i)$, and $b_k = b_0 + \eta \sum_{i=0}^k f(b_i)$. We can see now if $f(u) = c$, $0 < c < 1$, then as $k \rightarrow \infty$, the bounds $a_k \rightarrow -\infty$, $b_k \rightarrow \infty$. This leads to the claimed divergence.

To solve the issue of bounds diverging we propose the following formulations for one dimensional bounds, and then we extend them to n - dimensions, which allows for finding the n -dimensional semantic robust/adversarial regions that are similar to figure 2. some of the formulations are black-box in nature (they dont need the gradient of the function f in order to update the current estimates of the bound) while others .

B.3 Naive Approach

$$L = -\text{Area}_{\text{in}} + \frac{\lambda}{2} |b - a|_2^2 \quad (24)$$

using Libeniz rule as in Lemma 1, we get the following update steps for the objective L :

$$\begin{aligned} \frac{\partial L}{\partial a} &= f(a) - \lambda(b - a) \\ \frac{\partial L}{\partial b} &= -f(b) + \lambda(b - a) \end{aligned} \quad (25)$$

where λ is regularizing the boundaries not to extend too much in the case the function evaluation wa positive all the time.

Extension to n -dimension: Lets start by $n = 2$. Now, we have $f : \mathbb{R}^2 \rightarrow (0, 1)$, then we define the loss integral as a function of four bounds of a rectangular region as follows.

$$\begin{aligned} L(a_1, a_2, b_1, b_2) &= \\ &= - \int_{a_2}^{b_2} \int_{a_1}^{b_1} f(u, v) dv du + \frac{\lambda}{2} |b_1 - a_1|_2^2 + \frac{\lambda}{2} |b_2 - a_2|_2^2 \end{aligned} \quad (26)$$

We apply the trapezoidal approximation on the loss to obtain the following expression.

$$\begin{aligned}
L(a_1, a_2, b_1, b_2) &\approx \frac{\lambda}{2} |b_1 - a_1|_2^2 + \frac{\lambda}{2} |b_2 - a_2|_2^2 \\
&\quad - \frac{(b_1 - a_1)(b_2 - a_2)}{4} (f(a_1, a_2) + f(b_1, a_2) + \\
&\quad\quad\quad f(a_1, b_2) + f(b_1, b_2))
\end{aligned} \tag{27}$$

to find the update direction for the first bound a_1 by taking the partial derivative of the function in Eq (26) we get the following update direction for a_1 along with its trapezoidal approximation in order to able to compute it during the optimization:

$$\begin{aligned}
\frac{\partial L}{\partial a_1} &= \int_{a_2}^{b_2} f(a_1, v) dv - \lambda(b_1 - a_1) \\
&\approx \frac{(b_2 - a_2)}{2} (f(a_1, a_2) + f(a_1, b_2)) - \lambda(b_1 - a_1)
\end{aligned} \tag{28}$$

Doing similar steps to the first bound for the other three bounds we obtain the full update directions for (a_1, a_2, b_1, b_2)

$$\begin{aligned}
\frac{\partial L}{\partial a_1} &\approx \frac{(b_2 - a_2)}{2} (f(a_1, a_2) + f(a_1, b_2)) - \lambda(b_1 - a_1) \\
\frac{\partial L}{\partial b_1} &\approx -\frac{(b_2 - a_2)}{2} (f(b_1, a_2) + f(b_1, b_2)) + \lambda(b_1 - a_1) \\
\frac{\partial L}{\partial a_2} &\approx \frac{(b_1 - a_1)}{2} (f(a_1, a_2) + f(b_1, a_2)) - \lambda(b_2 - a_2) \\
\frac{\partial L}{\partial b_2} &\approx -\frac{(b_1 - a_1)}{2} (f(a_1, b_2) + f(b_1, b_2)) + \lambda(b_2 - a_2)
\end{aligned} \tag{29}$$

Now, for $f : \mathbb{R}^n \rightarrow (0, 1)$, we define the inner region hyper-rectangle as before $\mathbb{D} = \{\mathbf{x} : \mathbf{a} \leq \mathbf{x} \leq \mathbf{b}\}$. Here, we assume the size of the region is positive at every dimension, *i.e.* $\mathbf{r} = \mathbf{b} - \mathbf{a} > \mathbf{0}$. The volume of the region \mathbb{D} normalized by exponent of dimension n is expressed as follows

$$\text{volume}(\mathbb{D}) = \Delta = \frac{1}{2^n} \prod_{i=1}^n \mathbf{r}_i \tag{30}$$

The region \mathbb{D} can also be defined in terms of the matrix \mathbf{D} of all the corner points $\{\mathbf{d}^i\}_{i=1}^{2^n}$ as follows.

$$\begin{aligned}
\text{corners}(\mathbb{D}) &= \mathbf{D}_{n \times 2^n} = [\mathbf{d}^1 | \mathbf{d}^2 | \dots | \mathbf{d}^{2^n}] \\
\mathbf{D} &= \mathbf{1}^T \mathbf{a} + \mathbf{M}^T \odot (\mathbf{1}^T \mathbf{r})
\end{aligned} \tag{31}$$

where $\mathbf{1}$ is the all-ones vector of size 2^n , \odot is the Hadamard product of matrices (element-wise), and \mathbf{M} is a constant masking matrix defined as the

matrix of binary numbers of n bits that range from 0 to $2^n - 1$ defined as follows.

$$\mathbf{M}_{n \times 2^n} = [\mathbf{m}^0 | \mathbf{m}^1 | \dots | \mathbf{m}^{2^n - 1}] , \text{ where } \mathbf{m}^i = \text{binary}_n(i) \quad (32)$$

We define the function vector as the vector $\mathbf{f}_{\mathbb{D}}$ of all function evaluations at all corner points of \mathbb{D}

$$\mathbf{f}_{\mathbb{D}} = [f(\mathbf{d}^1), f(\mathbf{d}^2), \dots, f(\mathbf{d}^{2^n})]^T , \mathbf{d}^i = \mathbf{D}_{:,i} \quad (33)$$

We follow similar steps as in $n = 2$ and obtain the following loss expressions and update directions :

$$\begin{aligned} L(\mathbf{a}, \mathbf{b}) &= - \int \dots \int_{\mathbb{D}} f(u_1, \dots, u_n) du_1 \dots du_n + \frac{\lambda}{2} |\mathbf{r}|^2 \\ &\approx -\Delta \mathbf{1}^T \mathbf{f}_{\mathbb{D}} + \frac{\lambda}{2} |\mathbf{r}|^2 \\ \nabla_{\mathbf{a}} L &\approx 2\Delta \text{diag}^{-1}(\mathbf{r}) \bar{\mathbf{M}} \mathbf{f}_{\mathbb{D}} + \lambda \mathbf{r} \\ \nabla_{\mathbf{b}} L &\approx -2\Delta \text{diag}^{-1}(\mathbf{r}) \mathbf{M} \mathbf{f}_{\mathbb{D}} - \lambda \mathbf{r} \end{aligned} \quad (34)$$

B.4 Outer-Inner Ratio Loss (OIR)

We introduce an outer region A, B with bigger area that contains the small region (a, b) . We follow the following assumption to insure that outer area is always positive.

$$A = a - \alpha \frac{b-a}{2}, B = b + \alpha \frac{b-a}{2} \quad (35)$$

where α is the small boundary factor of the outer area to inner area. We formulate the problem as a ratio of outer over inner area and we try to make this ratio as close as possible to 0 . $L = \frac{\text{Area}_{\text{out}}}{\text{Area}_{\text{in}}}$ By using DencklBeck technique for solving non-linear fractional programming problems [31]. Using their formulation to transform L as follows.

$$\begin{aligned} L &= \frac{\text{Area}_{\text{out}}}{\text{Area}_{\text{in}}} = \text{Area}_{\text{out}} - \lambda \text{Area}_{\text{in}} \\ &= \int_A^B f(a) du - \int_a^b f(a) du - \lambda \int_a^b f(a) du \end{aligned} \quad (36)$$

where $\lambda^* = \frac{\text{Area}_{\text{out}}^*}{\text{Area}_{\text{in}}^*}$ is the DencklBeck factor and it is equal to the small objective best achieved.

Black-Box (OIR_B).

Here we set $\lambda = 1$ to simplify the problem. This yields the following expression of the loss

$$\begin{aligned}
L &= \text{Area}_{\text{out}} - \text{Area}_{\text{in}} \\
&= \int_A^a f(u)du + \int_b^B f(u)du - \int_a^b f(u)du \\
&= \int_A^B f(u)du - 2 \int_a^b f(u)du \\
&= \int_{a-\alpha\frac{b-a}{2}}^{b+\alpha\frac{b-a}{2}} f(u)du - 2 \int_a^b f(u)du
\end{aligned} \tag{37}$$

using Libeniz rule as in Lemma 1, we get the following update steps for the objective L :

$$\begin{aligned}
\frac{\partial L}{\partial a} &= -\left(1 + \frac{\alpha}{2}\right)f(A) - \frac{\alpha}{2}f(B) + 2f(a) \\
\frac{\partial L}{\partial b} &= \left(1 + \frac{\alpha}{2}\right)f(B) + \frac{\alpha}{2}f(A) - 2f(b)
\end{aligned} \tag{38}$$

Extension to n-dimension:. Lets start by $n = 2$. Now, we have $f : \mathbb{R}^2 \rightarrow (0, 1)$, and with the following constrains on the outer region.

$$\begin{aligned}
A_1 &= a_1 - \frac{b_1 - a_1}{2}, & B_1 &= b_1 + \frac{b_1 - a_1}{2} \\
A_2 &= a_2 - \frac{b_2 - a_2}{2}, & B_2 &= b_2 + \frac{b_2 - a_2}{2}
\end{aligned} \tag{39}$$

we define the loss integral as a function of four bounds of a rectangular region as follows.

$$\begin{aligned}
L(a_1, a_2, b_1, b_2) &= \\
&\int_{A_2}^{B_2} \int_{A_1}^{B_1} f(u, v)dvdu - 2 \int_{a_2}^{b_2} \int_{a_1}^{b_1} f(u, v)dvdu
\end{aligned} \tag{40}$$

We apply the trapezoidal approximation on the loss to obtain the following expression.

$$\begin{aligned}
L(a_1, a_2, b_1, b_2) &\approx \\
&\frac{(B_1 - A_1)(B_2 - A_2)}{4} (f(A_1, A_2) + f(B_1, A_2) + \\
&\quad f(A_1, B_2) + f(B_1, B_2)) \\
&- \frac{(b_1 - a_1)(b_2 - a_2)}{2} (f(a_1, a_2) + f(b_1, a_2) + \\
&\quad f(a_1, b_2) + f(b_1, b_2)) \\
&= \frac{(b_1 - a_1)(b_2 - a_2)}{4} (\\
&\quad (1 + \alpha)^2 (f(A_1, A_2) + f(B_1, A_2) + \\
&\quad f(A_1, B_2) + f(B_1, B_2)) \\
&\quad - 2 (f(a_1, a_2) + f(b_1, a_2) + f(a_1, b_2) + f(b_1, b_2)))
\end{aligned} \tag{41}$$

to find the update direction for the first bound a_1 by taking the partial derivative of the function in Eq (40) we get the following update direction for a_1 along with its trapezoidal approximation in order to able to compute it during the optimization:

$$\begin{aligned}
\frac{\partial L}{\partial a_1} &= -(1 + \frac{\alpha}{2}) \int_{A_2}^{B_2} \left(f(A_1, v) + \frac{\alpha}{2} f(B_1, v) \right) dv \\
&+ 2 \int_{a_2}^{b_2} f(a_1, v) dv \\
&\approx \frac{(b_2 - a_2)}{2} (\\
&\quad - (1 + \alpha) \left(\left(1 + \frac{\alpha}{2} \right) (f(A_1, A_2) + f(A_1, B_2)) \right. \\
&\quad \quad \quad \left. + \frac{\alpha}{2} (f(B_1, A_2) + f(B_1, B_2)) \right) \\
&\quad \left. + 2 \left(f(a_1, a_2) + f(a_1, b_2) \right) \right)
\end{aligned} \tag{42}$$

Doing similar steps to the first bound for the other three bounds we obtain the full update directions for (a_1, a_2, b_1, b_2)

$$\begin{aligned}
\frac{\partial L}{\partial a_1} &\approx \frac{(b_2 - a_2)}{2} (\\
&\quad - (1 + \alpha) \left(\left(1 + \frac{\alpha}{2} \right) (f(A_1, A_2) + f(A_1, B_2)) \right. \\
&\quad \quad \quad \left. + \frac{\alpha}{2} (f(B_1, A_2) + f(B_1, B_2)) \right) \\
&\quad \left. + 2 \left(f(a_1, a_2) + f(a_1, b_2) \right) \right)
\end{aligned} \tag{43}$$

$$\begin{aligned}
\frac{\partial L}{\partial b_1} &\approx \frac{(b_2 - a_2)}{2} (\\
&\quad (1 + \alpha) \left(\left(1 + \frac{\alpha}{2} \right) (f(B_1, A_2) + f(B_1, B_2)) \right) \\
&\quad \quad \quad + \frac{\alpha}{2} (f(A_1, A_2) + f(A_1, B_2)) \\
&\quad \left. - 2 \left(f(b_1, a_2) + f(b_1, b_2) \right) \right)
\end{aligned} \tag{44}$$

$$\begin{aligned}
\frac{\partial L}{\partial a_2} &\approx \frac{(b_1 - a_1)}{2} (\\
&\quad - (1 + \alpha) \left(\left(1 + \frac{\alpha}{2} \right) (f(A_1, A_2) + f(B_1, A_2)) \right. \\
&\quad \quad \quad \left. + \frac{\alpha}{2} (f(A_1, B_2) + f(B_1, B_2)) \right) \\
&\quad \left. + 2 \left(f(a_1, a_2) + f(b_1, a_2) \right) \right)
\end{aligned} \tag{45}$$

$$\begin{aligned}
\frac{\partial L}{\partial b_2} \approx & \frac{(b_1 - a_1)}{2} \left(\right. \\
& (1 + \alpha) \left(1 + \frac{\alpha}{2} \right) (f(A_1, B_2) + f(B_1, B_2)) \\
& + \frac{\alpha}{2} (f(A_1, A_2) + f(B_1, A_2)) \left. \right) \\
& - 2 \left(f(a_1, b_2) + f(b_1, b_2) \right) \left. \right)
\end{aligned} \tag{46}$$

Now, for $f : \mathbb{R}^n \rightarrow (0, 1)$, we define the inner region hyper-rectangle as before $\mathbb{D} = \{\mathbf{x} : \mathbf{a} \leq \mathbf{x} \leq \mathbf{b}\}$, but now define an outer bigger region \mathbb{Q} that include the smaller region \mathbb{D} and defined as follows : $\mathbb{Q} = \{\mathbf{x} : \mathbf{a} - \frac{\alpha}{2}\mathbf{r} \leq \mathbf{x} \leq \mathbf{b} + \frac{\alpha}{2}\mathbf{r}\}$, where $\mathbf{a}, \mathbf{b}, \mathbf{r}$ are defined as before, while α is defined as the boundary factor of the outer region in all the dimensions equivilantly. The inner and outer regions can also be defined in terms of the corner points as follows.

$$\begin{aligned}
\text{corners}(\mathbb{D}) &= \mathbf{D}_{n \times 2^n} = \left[\mathbf{d}^1 | \mathbf{d}^2 | \dots | \mathbf{d}^{2^n} \right] \\
\mathbf{D} &= \mathbf{1}^T \mathbf{a} + \mathbf{M}^T \odot (\mathbf{1}^T \mathbf{r}) \\
\text{corners}(\mathbb{Q}) &= \mathbf{Q}_{n \times 2^n} = \left[\mathbf{q}^1 | \mathbf{q}^2 | \dots | \mathbf{q}^{2^n} \right] \\
\mathbf{Q} &= \mathbf{1}^T \left(\mathbf{a} - \frac{\alpha}{2} \mathbf{r} \right) + (1 + \alpha) \mathbf{M}^T \odot (\mathbf{1}^T \mathbf{r})
\end{aligned} \tag{47}$$

where $\mathbf{1}$ is the all-ones vector of size 2^n , \odot is the Hadamard product of matrices (elemnt-wise), and \mathbf{M} is a constant masking matrix defined in Eq (32). Now we define two function vectors evaluated at all possible inner and outer corner points respectively.

$$\begin{aligned}
\mathbf{f}_{\mathbb{D}} &= \left[f(\mathbf{d}^1), f(\mathbf{d}^2), \dots, f(\mathbf{d}^{2^n}) \right]^T, \mathbf{d}^i = \mathbf{D}_{:,i} \\
\mathbf{f}_{\mathbb{Q}} &= \left[f(\mathbf{q}^1), f(\mathbf{q}^2), \dots, f(\mathbf{q}^{2^n}) \right]^T, \mathbf{c}^i = \mathbf{Q}_{:,i}
\end{aligned} \tag{48}$$

Now the loss and update directions for the n-dimensional case becomes as follows

$$\begin{aligned}
L(\mathbf{a}, \mathbf{b}) &= \int \dots \int_{\mathbb{Q}} f(u_1, \dots, u_n) du_1 \dots du_n \\
&\quad - 2 \int \dots \int_{\mathbb{D}} f(u_1, \dots, u_n) du_1 \dots du_n \\
&\approx \Delta \left((1 + \alpha)^n \mathbf{1}^T \mathbf{f}_{\mathbb{Q}} - 2 \mathbf{1}^T \mathbf{f}_{\mathbb{D}} \right) \\
\nabla_{\mathbf{a}} L &\approx 2 \Delta \text{diag}^{-1}(\mathbf{r}) \left(2 \overline{\mathbf{M}} \mathbf{f}_{\mathbb{D}} - \overline{\mathbf{M}}_{\mathbb{Q}} \mathbf{f}_{\mathbb{Q}} \right) \\
\nabla_{\mathbf{b}} L &\approx 2 \Delta \text{diag}^{-1}(\mathbf{r}) \left(-2 \mathbf{M} \mathbf{f}_{\mathbb{D}} + \mathbf{M}_{\mathbb{Q}} \mathbf{f}_{\mathbb{Q}} \right)
\end{aligned} \tag{49}$$

where $\overline{\mathbf{M}}_{\mathbb{Q}}$ is the outer region mask defined as follows.

$$\begin{aligned}
\overline{\mathbf{M}}_{\mathbb{Q}} &= (1 + \alpha)^{n-1} \left(\left(1 + \frac{\alpha}{2} \right) \overline{\mathbf{M}} + \frac{\alpha}{2} \mathbf{M} \right) \\
\mathbf{M}_{\mathbb{Q}} &= (1 + \alpha)^{n-1} \left(\left(1 + \frac{\alpha}{2} \right) \mathbf{M} + \frac{\alpha}{2} \overline{\mathbf{M}} \right)
\end{aligned} \tag{50}$$

White-Box OIR (OIR_W.) The following formulation is white-box in nature (it need the gradient of the function f in order to update the current estimates of the bound) this is useful when the function in hand is differntiable (*e.g.* DNN) , to obtain more intelligent regions, rather then the regions surrounded by near 0 values of the function f . We set $\lambda = \frac{\alpha}{\beta}$ in Eq (36), where α is the small boundary factor of the outer area, β is the emphasis factor (we will show later how it determines the emphasis on the function vs the gradient). Hence, the objective in Eq (36) becomes :

$$\begin{aligned} \arg \min_{a,b} L &= \arg \min_{a,b} \text{Area}_{\text{out}} - \lambda \text{Area}_{\text{in}} \\ &= \arg \min_{a,b} \int_A^a f(u)du + \int_b^B f(u)du - \frac{\alpha}{\beta} \int_a^b f(u)du \\ &= \arg \min_{a,b} \frac{\beta}{\alpha} \int_{a-\alpha\frac{b-a}{2}}^{b+\alpha\frac{b-a}{2}} f(u)du - (1 + \frac{\beta}{\alpha}) \int_a^b f(u)du \end{aligned} \quad (51)$$

using Libeniz rule as in Lemma 1, we get the following derivatives of the bound a :

$$\begin{aligned} \frac{\partial L}{\partial a} &= \frac{\beta}{\alpha} \left(f(a) - f\left(a - \alpha\frac{b-a}{2}\right) \right) \\ &\quad - \frac{\beta}{2} f\left(b + \alpha\frac{b-a}{2}\right) - \frac{\beta}{2} f\left(a - \alpha\frac{b-a}{2}\right) + f(a) \end{aligned} \quad (52)$$

now since λ^* should be small for the optimal objective , then as $\lambda \rightarrow 0$, $\alpha \rightarrow 0$ and hence the derivative in Eq (52) becomes the following.

$$\begin{aligned} \lim_{\alpha \rightarrow 0} \frac{\partial L}{\partial a} &= \lim_{\alpha \rightarrow 0} \beta \frac{\left(f(a) - f\left(a - \alpha\frac{b-a}{2}\right) \right)}{\alpha} \\ &\quad - \frac{\beta}{2} f(b) - \frac{\beta}{2} f(a) + f(a) \end{aligned} \quad (53)$$

We can see that the first term is proportional to the derivative of f at a , and hence the expression becomes :

$$\lim_{\alpha \rightarrow 0} \frac{\partial L}{\partial a} = \frac{\beta}{2} \left((b-a)f'(a) + f(b) \right) + \left(1 - \frac{\beta}{2}\right) f(a) \quad (54)$$

we can see that the update rule depends on the function value and the derivative of f at the boundary a with β controlling the dependence. Similarly for the boundary b we can see the following direction

$$\lim_{\alpha \rightarrow 0} \frac{\partial L}{\partial b} = \frac{\beta}{2} \left((b-a)f'(b) + f(a) \right) - \left(1 - \frac{\beta}{2}\right) f(b) \quad (55)$$

If $\beta \rightarrow 0$, the update directions in Eq (54,55) collapse to the unregularized naive update in Eq (25) .

Extension to n-dimension.. Lets start by $n = 2$. Now, we have $f : \mathbb{R}^2 \rightarrow (0, 1)$, and with the following constrains on the outer region.

$$\begin{aligned} A_1 &= a_1 - \frac{b_1 - a_1}{2}, & B_1 &= b_1 + \frac{b_1 - a_1}{2} \\ A_2 &= a_2 - \frac{b_2 - a_2}{2}, & B_2 &= b_2 + \frac{b_2 - a_2}{2} \end{aligned} \quad (56)$$

we follow similar approach as in Eq (51) to obtain the following expression.

$$\begin{aligned} L(a_1, a_2, b_1, b_2) &= \\ \frac{\beta}{\alpha} \int_{A_2}^{B_2} \int_{A_1}^{B_1} f(u, v) dv du &- \left(1 + \frac{\beta}{\alpha}\right) \int_{a_2}^{b_2} \int_{a_1}^{b_1} f(u, v) dv du \end{aligned} \quad (57)$$

We apply the trapezoidal approximation on the loss to obtain the following approximation.

$$\begin{aligned} L(a_1, a_2, b_1, b_2) &\approx -1 + (1 + \alpha)^2 \\ &\frac{(f(A_1, A_2) + f(B_1, A_2) + f(A_1, B_2) + f(B_1, B_2))}{(f(a_1, a_2) + f(b_1, a_2) + f(a_1, b_2) + f(b_1, b_2))} \end{aligned} \quad (58)$$

to find the update direction for the first bound a_1 by taking the partial derivative of the function in Eq (40) we get the following update direction for a_1 along with its trapezoidal approximation in order to able to compute it during the optimization:

$$\begin{aligned} \frac{\partial L}{\partial a_1} &= -\frac{\beta}{\alpha} \left(1 + \frac{\alpha}{2}\right) \int_{A_2}^{B_2} \left(f(A_1, v) + \frac{\alpha}{2} f(B_1, v)\right) dv \\ &\quad + \left(1 + \frac{\beta}{\alpha}\right) \int_{a_2}^{b_2} f(a_1, v) dv \\ &\approx \frac{(b_2 - a_2)}{2} \left(\right. \\ &\quad - (1 + \alpha) \left(\frac{\beta}{\alpha} + \frac{\beta}{2} \right) (f(A_1, A_2) + f(A_1, B_2)) \\ &\quad \quad \quad \left. + \frac{\beta}{2} (f(B_1, A_2) + f(B_1, B_2)) \right) \\ &\quad + \left(1 + \frac{\beta}{\alpha}\right) \left(f(a_1, a_2) + f(a_1, b_2) \right) \end{aligned} \quad (59)$$

grouping the terms which are divided by α together and then taking the limit of $\alpha \rightarrow \infty$ (as explained in the 1-d case), we get the following expressions.

$$\begin{aligned}
\lim_{\alpha \rightarrow 0} \frac{\partial L}{\partial a_1} &\approx \frac{(b_2 - a_2)}{2} (\\
\lim_{\alpha \rightarrow 0} \frac{\beta}{\alpha} &((f(a_1, a_2) + f(a_1, b_2)) - (f(A_1, A_2) + f(A_1, B_2))) \\
&- \lim_{\alpha \rightarrow 0} \frac{3\beta}{2} (f(A_1, A_2) + f(A_1, B_2)) \\
&- \lim_{\alpha \rightarrow 0} \frac{\beta}{2} (f(B_1, A_2) + f(B_1, B_2)) \\
&+ (f(a_1, a_2) + f(a_1, b_2)))
\end{aligned} \tag{60}$$

Noting that the first term is related to the directional derivatives of f , we get the following limit expression

$$\begin{aligned}
\lim_{\alpha \rightarrow 0} \frac{\partial L}{\partial a_1} &\approx \frac{(b_2 - a_2)}{2} (\\
\beta (\nabla f(a_1, a_2) \cdot (\frac{b_1 - a_1}{2}, \frac{b_2 - a_2}{2}) + \nabla f(a_1, b_2) \cdot (\frac{b_1 - a_1}{2}, -\frac{b_2 - a_2}{2})) \\
&+ (1 - \frac{3\beta}{2}) (f(a_1, a_2) + f(a_1, b_2))) \\
&- \frac{\beta}{2} (f(b_1, a_2) + f(b_1, b_2))
\end{aligned} \tag{61}$$

Doing similar steps to the first bound for the other three bounds we obtain the full update directions for (a_1, a_2, b_1, b_2)

$$\begin{aligned}
\lim_{\alpha \rightarrow 0} \frac{\partial L}{\partial a_1} &\approx \frac{(b_2 - a_2)}{2} (\\
\beta (\nabla f(a_1, a_2) \cdot (\frac{b_1 - a_1}{2}, \frac{b_2 - a_2}{2}) + \nabla f(a_1, b_2) \cdot (\frac{b_1 - a_1}{2}, -\frac{b_2 - a_2}{2})) \\
&+ (1 - \frac{3\beta}{2}) (f(a_1, a_2) + f(a_1, b_2))) \\
&- \frac{\beta}{2} (f(b_1, a_2) + f(b_1, b_2))
\end{aligned} \tag{62}$$

$$\begin{aligned}
\lim_{\alpha \rightarrow 0} \frac{\partial L}{\partial b_1} &\approx \frac{(b_2 - a_2)}{2} (\\
\beta (\nabla f(b_1, a_2) \cdot (\frac{b_1 - a_1}{2}, -\frac{b_2 - a_2}{2}) + \nabla f(b_1, b_2) \cdot (\frac{b_1 - a_1}{2}, \frac{b_2 - a_2}{2})) \\
&- (1 - \frac{3\beta}{2}) (f(b_1, a_2) + f(b_1, b_2))) \\
&+ \frac{\beta}{2} (f(a_1, a_2) + f(a_1, b_2))
\end{aligned} \tag{63}$$

$$\begin{aligned}
\lim_{\alpha \rightarrow 0} \frac{\partial L}{\partial a_2} &\approx \frac{(b_2 - a_2)}{2} \left(\right. \\
&\beta \left(\nabla f(a_1, a_2) \cdot \begin{pmatrix} (b_1 - a_1) \\ (b_2 - a_2) \end{pmatrix} + \nabla f(b_1, a_2) \cdot \begin{pmatrix} -(b_1 - a_1) \\ (b_2 - a_2) \end{pmatrix} \right) \\
&+ \left(1 - \frac{3\beta}{2} \right) \left(f(a_1, a_2) + f(b_1, a_2) \right) \\
&\left. - \frac{\beta}{2} \left(f(a_1, b_2) + f(b_1, b_2) \right) \right)
\end{aligned} \tag{64}$$

$$\begin{aligned}
\lim_{\alpha \rightarrow 0} \frac{\partial L}{\partial b_2} &\approx \frac{(b_2 - a_2)}{2} \left(\right. \\
&\beta \left(\nabla f(a_1, b_2) \cdot \begin{pmatrix} -(b_1 - a_1) \\ (b_2 - a_2) \end{pmatrix} + \nabla f(a_2, b_2) \cdot \begin{pmatrix} (b_1 - a_1) \\ (b_2 - a_2) \end{pmatrix} \right) \\
&- \left(1 - \frac{3\beta}{2} \right) \left(f(a_1, b_2) + f(b_1, b_2) \right) \\
&+ \frac{\beta}{2} \left(f(a_1, a_2) + f(b_1, a_2) \right)
\end{aligned} \tag{65}$$

Now, for $f : \mathbb{R}^n \rightarrow (0, 1)$ Following previous notations we have the following expressions for the loss and update directions for the bound

$$\begin{aligned}
L(\mathbf{a}, \mathbf{b}) &\approx \frac{(1 + \alpha)^n \mathbf{1}^T \mathbf{f}_{\mathbb{Q}}}{\mathbf{1}^T \mathbf{f}_{\mathbb{D}}} - 1 \\
\nabla_{\mathbf{a}} L &\approx \Delta \left(\text{diag}^{-1}(\mathbf{r}) \overline{\mathbf{M}}_{\mathbb{D}} \mathbf{f}_{\mathbb{D}} + \beta \text{diag}(\overline{\mathbf{M}} \mathbf{G}_{\mathbb{D}}) + \beta \overline{\mathbf{s}} \right) \\
\nabla_{\mathbf{b}} L &\approx \Delta \left(-\text{diag}^{-1}(\mathbf{r}) \mathbf{M}_{\mathbb{D}} \mathbf{f}_{\mathbb{D}} + \beta \text{diag}(\mathbf{M} \mathbf{G}_{\mathbb{D}}) + \beta \mathbf{s} \right)
\end{aligned} \tag{66}$$

where the mask is the special mask

$$\begin{aligned}
\overline{\mathbf{M}}_{\mathbb{D}} &= \left(\gamma_n \overline{\mathbf{M}} - \beta \mathbf{M} \right) \\
\mathbf{M}_{\mathbb{D}} &= \left(\gamma_n \mathbf{M} - \beta \overline{\mathbf{M}} \right) \\
\gamma_n &= 2 - \beta(2n - 1)
\end{aligned} \tag{67}$$

Where $\text{diag}(\cdot)$ is the diagonal matrix of the vector argument or the diagonal vector of the matrix argument. \mathbf{s} is a weighted sum of the gradient from other dominions ($i \neq k$) contributing to the update direction of dimension k , where $k \in \{1, 2, \dots, n\}$.

$$\begin{aligned}
\mathbf{s}_k &= \frac{1}{\mathbf{r}_k} \sum_{i=1, i \neq k}^n \mathbf{r}_i \left((\overline{\mathbf{M}}_{i,:} - \mathbf{M}_{i,:}) \odot \overline{\mathbf{M}}_{k,:} \right) \mathbf{G}_{:,i} \\
\overline{\mathbf{s}}_k &= \frac{1}{\mathbf{r}_k} \sum_{i=1, i \neq k}^n \mathbf{r}_i \left((\mathbf{M}_{i,:} - \overline{\mathbf{M}}_{i,:}) \odot \mathbf{M}_{k,:} \right) \mathbf{G}_{:,i} \\
k &\in \{1, 2, \dots, n\}
\end{aligned} \tag{68}$$

B.5 Trapezoidal Approximation Formulation

Here we use the trapezoidal approximation of the integral, a first-order approximation from Newton-Cotes formulas for numerical integration [36]. The rule states that a definite integral can be approximated as follows:

$$\int_a^b f(u)du \approx (b-a) \frac{f(a) + f(b)}{2} \quad (69)$$

asymptotic error estimate is given by $-\frac{(b-a)^2}{48} [f'(b) - f'(a)] + \mathcal{O}(0.125)$. So as long the derivatives are bounded by some lipschitz constant \mathbb{L} , then the error becomes bounded by the following $|\text{error}| \leq \mathbb{L}(b-a)^2$. The regularized loss of interest in Eq (24) becomes the following .

$$\begin{aligned} L &= -\text{Area}_{\text{in}} + \lambda |b-a|_2^2 \\ &\approx -(b-a) \frac{f(a) + f(b)}{2} + \lambda |b-a|_2^2 \end{aligned} \quad (70)$$

taking the derivative of L approximation directly with respect to these bounds , yields the following update directions which are different from the expressions in Eq (25)

$$\begin{aligned} \frac{\partial L}{\partial a} &= -\frac{b-a}{2} f'(a) + \frac{f(a) + f(b)}{2} - \lambda(b-a) \\ \frac{\partial L}{\partial b} &= -\frac{b-a}{2} f'(b) - \frac{f(a) + f(b)}{2} + \lambda(b-a) \end{aligned} \quad (71)$$

note that it needs the first derivative $f'(\cdot)$ of the function f evaluated at the bound to update that bound.

Extension to n-dimensions.

Lets start by $n = 2$. Now, we have $f : \mathbb{R}^2 \rightarrow (0, 1)$, and we define the loss integral as a function of four bounds of a rectangular region and apply the trapezoidal approximation as follows.

$$\begin{aligned} L(a_1, a_2, b_1, b_2) &= - \int_{a_1}^{b_1} \int_{a_2}^{b_2} f(u, v) dv du \\ &\quad + \frac{\lambda}{2} |b_1 - a_1|_2^2 + \frac{\lambda}{2} |b_2 - a_2|_2^2 \\ &\approx \frac{\lambda}{2} |b_1 - a_1|_2^2 + \frac{\lambda}{2} |b_2 - a_2|_2^2 \\ &\quad - \frac{(b_1 - a_1)(b_2 - a_2)}{4} \left(f(a_1, a_2) + f(b_1, a_2) + \right. \\ &\quad \left. f(a_1, b_2) + f(b_1, b_2) \right) \end{aligned} \quad (72)$$

Then following similar steps as in the one-dimensional case we can obtain the following update directions for the four bounds

$$\begin{aligned} \frac{\partial L}{\partial a_1} &= (b_1 - a_1)(b_2 - a_2) \frac{f'_1(a_1, a_2) + f'_1(a_1, b_2)}{4} \\ &\quad - (b_2 - a_2) \frac{f(a_1, a_2) + f(a_1, b_2) + f(b_1, a_2) + f(b_1, b_2)}{4} \\ &\quad - \lambda(b_1 - a_1) \end{aligned} \quad (73)$$

$$\begin{aligned} \frac{\partial L}{\partial a_2} &= (b_1 - a_1)(b_2 - a_2) \frac{f'_2(b_1, a_2) + f'_2(b_1, b_2)}{4} \\ &\quad - (b_2 - a_2) \frac{f(a_1, a_2) + f(a_1, b_2) + f(b_1, a_2) + f(b_1, b_2)}{4} \\ &\quad - \lambda(b_2 - a_2) \end{aligned} \quad (74)$$

$$\begin{aligned} \frac{\partial L}{\partial b_1} &= (b_1 - a_1)(b_2 - a_2) \frac{f'_1(a_1, a_2) + f'_1(b_1, a_2)}{4} \\ &\quad + (b_1 - a_1) \frac{f(a_1, a_2) + f(a_1, b_2) + f(b_1, a_2) + f(b_1, b_2)}{4} \\ &\quad + \lambda(b_1 - a_1) \end{aligned} \quad (75)$$

$$\begin{aligned} \frac{\partial L}{\partial b_2} &= (b_1 - a_1)(b_2 - a_2) \frac{f'_2(a_1, b_2) + f'_2(b_1, b_2)}{4} \\ &\quad + (b_1 - a_1) \frac{f(a_1, a_2) + f(a_1, b_2) + f(b_1, a_2) + f(b_1, b_2)}{4} \\ &\quad + \lambda(b_2 - a_2) \end{aligned} \quad (76)$$

Where $f'_1(\cdot) = \frac{\partial f(u,v)}{\partial u}$, $f'_2(\cdot) = \frac{\partial f(u,v)}{\partial v}$. extending the 2-dimensional to general n -dimensions is straight forward. For $f : \mathbb{R}^n \rightarrow (0, 1)$, we define the following. Let the left bound vector be $\mathbf{a} = [a_1, a_2, \dots, a_n]$ and the right bound vector $\mathbf{b} = [b_1, b_2, \dots, b_n]$ define the n -dimensional hyper-rectangle region of interest. The region is then defined as follows : $\mathbb{D} = \{\mathbf{x} : \mathbf{a} \leq \mathbf{x} \leq \mathbf{b}\}$, Here, we assume the size of the region is positive at every dimension, *i.e.* $\mathbf{r} = \mathbf{b} - \mathbf{a} > \mathbf{0}$. The volume of the region \mathbb{D} normalized by exponent of dimension n is expressed as in Eq (30), the region \mathbb{D} is defined as in Eq (31), \mathbf{M} is defined as in Eq (32), and $\mathbf{f}_{\mathbb{D}}$ is defined as in Eq (33). now we can see that the loss integral in Eq (72) becomes as follows .

$$\begin{aligned} L(\mathbf{a}, \mathbf{b}) &= \int \cdots \int_{\mathbb{D}} f(u_1, \dots, u_n) du_1 \dots du_n + \frac{\lambda}{2} |\mathbf{r}|^2 \\ &\approx \Delta \mathbf{1}^T \mathbf{f}_{\mathbb{D}} + \frac{\lambda}{2} |\mathbf{r}|^2 \end{aligned} \quad (77)$$

Similarly to Eq (33), we define the gradient matrix $\mathbf{G}_{\mathbb{D}}$ as the matrix of all gradient vectors evaluated at all corner points of \mathbb{D}

$$\mathbf{G}_{\mathbb{D}} = \left[\nabla f(\mathbf{d}^1) \mid \nabla f(\mathbf{d}^2) \mid \dots \mid \nabla f(\mathbf{d}^{2^n}) \right]^T \quad (78)$$

The update directions for the left bound \mathbf{a} and the right bound \mathbf{b} becomes as follows by the trapezoid approximation

$$\begin{aligned}\nabla_{\mathbf{a}}L &\approx \Delta\left(\text{diag}(\overline{\mathbf{M}}\mathbf{G}_{\mathbb{D}}) + \mathbf{1}^T\mathbf{f}_{\mathbb{D}}\text{diag}^{-1}(\mathbf{r})\mathbf{1}\right) + \lambda\mathbf{r} \\ \nabla_{\mathbf{b}}L &\approx \Delta\left(\text{diag}(\mathbf{M}\mathbf{G}_{\mathbb{D}}) - \mathbf{1}^T\mathbf{f}_{\mathbb{D}}\text{diag}^{-1}(\mathbf{r})\mathbf{1}\right) - \lambda\mathbf{r}\end{aligned}\tag{79}$$

Where $\overline{\mathbf{M}}$ is the complement of the binary mask matrix \mathbf{M} .

C Analysis

C.1 Detected Robust Regions

We apply the algorithms on two semantic parameters (the azimuth angle of the camera around the object, and the elevation angle around the object) that are regularly used in the literature [17,1]. When we use one parameter (the azimuth), we fix the elevation to 35° . We used two instead of larger numbers because it is easier to verify and visualize 2D, unlike higher dimensions. Also, the complexity of sampling increase exponentially with dimensionality for those algorithms (albeit being much better than grid sampling, see Table 3). The regions in Fig. 13,14 look vertical rectangles most of the time. This is because the scale of the horizontal-axis (0,360) is much smaller than the vertical axis (-10,90), so most regions are squares but looks rectangles because of figure scales.

C.2 hyper-parameters

How to select the hyper parameters in all the above algorithms? The answer is not straight forward. For the λ in the naive approach, it is set experimentally by trying different values and using the one which detects some regions that known to behave robustly. The values we found for this are $\lambda = 0.07 \sim 0.1$. The learning rate η is easier to detect with observing the convergence and depends on the full range of study. A rule of thumb is to make 0.001of the full range. For the OIR formulations, we have the boundary factor α which we set to 0.05. A rule of thumb is to set it to be between $0.5 \sim 1/N$, where N is the number of samples needed for that dimensions to adequately characterize the space. In our case $N = 180$, so $1/180 \approx 0.005$. The only hyperparameter with mathematically established bound is the emphasis factor of the OIR_W formulation β . The bound shown in Table 3 which is $0 \leq \beta \leq \frac{2}{2n-1}$ can be shown as follows. We start from Eq (67). This expression is the actual expression for the special masks (we apologize in the typos in the main paper). As we can see, the most important term is γ_n . IT dictates how the function at the boundaries determine the next move of the bounds. Here γ_n should always be positive to ensure the correct direction of the movement for positive function evaluation.

$$\begin{aligned} \gamma_n &> 0 \\ 2 - (2n - 1)\beta &> 0 \\ \beta &< \frac{2}{2n - 2} \end{aligned} \tag{80}$$

C.3 Detest

The data set used is collected from ShapeNet [7] and consists of 10 classes and 10 shapes each that are all identified by at least ResNet50 trained on ImagNet. This criteria is important to obtain valid NSM and DSM. The classes are ['aeroplane', 'bathtub', 'bench', 'bottle', 'chair', 'cup', 'piano', 'rifle', 'vase', 'toilet'].

Analysis Approach	Paradigm	Total Sampling complexity	Black-box Functions	Forward pass /step	Backward pass /step	Identification Capabaility
Grid Sampling	top-down	$\mathcal{O}(N^n)$ $N \gg 2$	✓	-	-	Fully identifies the semantic map of DNN
Naive	bottom-up	$\mathcal{O}(2^n)$	✓	2^n	0	finds strong robust regions only around \mathbf{u}_0
OIR_B	bottom-up	$\mathcal{O}(2^{n+1})$	✓	2^{n+1}	0	finds strong and weak robust regions around \mathbf{u}_0
OIR_W	bottom-up	$\mathcal{O}(2^n)$	✗	2^n	2^n	finds strong and weak robust regions around \mathbf{u}_0

Table 3: **Semantic Analysis Techniques:** comparing different approaches to analyse the semantic robustness of DNN.

Part of the dataset is shown in Fig. 11,12. 4 shapes faced difficulty of rendering during the SRVR experiments , therefore , they were replaced by another shapes from the same class.

C.4 Possible Future Directions

We analyze DNNs from a semantic lens and show how more confident networks tend to create adversarial semantic regions inside highly confident regions. We developed a bottom-up approach to analyzing the networks semantically by growing adversarial regions, which scales well with dimensionality and we use it to benchmark the semantic robustness of DNNs. We aim to investigate how to use the insights we gain from this work to develop and train semantically robust networks from the start while maintaining accuracy. Another direct extension of our work is to develop large scale semantic robustness challenge where we label these robust/adversarial regions in the semantic space and release some of them to allow for training. Then, we test the trained models on the hidden test set to measure robustness while reporting the accuracy on ImageNet validation set to make sure that the features of the model did not get affected by the robust training.

Algorithm 3: Robust n-dimensional Region Finding for Black-Box DNNs by Outer-Inner Ratios

Requires: Semantic Function of a DNN $f(\mathbf{u})$ in Eq (20), initial semantic parameter \mathbf{u}_0 , number of iterations T , learning rate η , object shape \mathbf{S}_z of class label z , boundary factor α , small ϵ

Form constant binary matrices $\mathbf{M}, \overline{\mathbf{M}}, \mathbf{M}_Q, \overline{\mathbf{M}}_Q, \mathbf{M}_D, \overline{\mathbf{M}}_D$

Initialize bounds $\mathbf{a}_0 \leftarrow \mathbf{u}_0 - \epsilon \mathbf{1}$, $\mathbf{b}_0 \leftarrow \mathbf{u}_0 + \epsilon \mathbf{1}$

$\mathbf{r}_0 \leftarrow \mathbf{a}_0 - \mathbf{b}_0$, update region volume Δ_0 as in Eq (30)

for $t \leftarrow 1$ **to** T **do**

- form the all-corners function vectors f_D, f_Q as in Eq (48)
- $\nabla_{\mathbf{a}} L \leftarrow 2\Delta_{t-1} \text{diag}^{-1}(\mathbf{r}_{t-1}) \left(2\overline{\mathbf{M}}\mathbf{f}_D - \overline{\mathbf{M}}_Q\mathbf{f}_Q \right)$
- $\nabla_{\mathbf{b}} L \leftarrow 2\Delta_{t-1} \text{diag}^{-1}(\mathbf{r}_{t-1}) \left(-2\mathbf{M}\mathbf{f}_D + \mathbf{M}_Q\mathbf{f}_Q \right)$
- update bounds: $\mathbf{a}_t \leftarrow \mathbf{a}_{t-1} - \eta \nabla_{\mathbf{a}} L$, $\mathbf{b}_t \leftarrow \mathbf{b}_{t-1} - \eta \nabla_{\mathbf{b}} L$
- $\mathbf{r}_t \leftarrow \mathbf{a}_t - \mathbf{b}_t$, update region volume Δ_t as in Eq (30)

end

Returns: robust region bounds: $\mathbf{a}_T, \mathbf{b}_T$.

Algorithm 4: Robust n-dimensional Region Finding for White-Box DNNs by Outer-Inner Ratios

Requires: Semantic Function of a DNN $f(\mathbf{u})$ in Eq (20), initial semantic parameter \mathbf{u}_0 , learning rate η , object shape \mathbf{S}_z of class label z , emphasis factor β , small ϵ

Form constant binary matrices $\mathbf{M}, \overline{\mathbf{M}}, \mathbf{M}_D, \overline{\mathbf{M}}_D$

Initialize bounds $\mathbf{a}_0 \leftarrow \mathbf{u}_0 - \epsilon \mathbf{1}$, $\mathbf{b}_0 \leftarrow \mathbf{u}_0 + \epsilon \mathbf{1}$

$\mathbf{r}_0 \leftarrow \mathbf{a}_0 - \mathbf{b}_0$, update region volume Δ_0 as in Eq (30)

for $t \leftarrow 1$ **to** T **do**

- form the all-corners function vector f_D as in Eq (48)
- form the all-corners gradients matrix \mathbf{G}_D as in Eq (78)
- form the gradient selection vectors $\mathbf{s}, \overline{\mathbf{s}}$ as in Eq (68)
- $\nabla_{\mathbf{a}} L \leftarrow \Delta_{t-1} \left(\text{diag}^{-1}(\mathbf{r}_{t-1}) \overline{\mathbf{M}}_D \mathbf{f}_D + \beta \text{diag}(\overline{\mathbf{M}} \mathbf{G}_D + \beta \overline{\mathbf{s}}) \right)$
- $\nabla_{\mathbf{b}} L \leftarrow \Delta_{t-1} \left(-\text{diag}^{-1}(\mathbf{r}_{t-1}) \mathbf{M}_D \mathbf{f}_D + \beta \text{diag}(\mathbf{M} \mathbf{G}_D) + \beta \mathbf{s} \right)$
- update bounds: $\mathbf{a}_t \leftarrow \mathbf{a}_{t-1} - \eta \nabla_{\mathbf{a}} L$, $\mathbf{b}_t \leftarrow \mathbf{b}_{t-1} - \eta \nabla_{\mathbf{b}} L$
- $\mathbf{r}_t \leftarrow \mathbf{a}_t - \mathbf{b}_t$, update region volume Δ_t as in Eq (30)

end

Returns: robust region bounds: $\mathbf{a}_T, \mathbf{b}_T$.
